Forschungszentrum Karlsruhe
Technik und Umwelt

Wissenschaftliche Berichte
FZKA 6679

Post-irradiation Studies on the (U, Pu)O_2 Cluster Experiment POUSSIX in the PHENIX Reactor

H. Kleykamp

Institut für Materialforschung
Programm Nukleare Sicherheitsforschung

Oktober 2001

Forschungszentrum Karlsruhe

Technik und Umwelt

Wissenschaftliche Berichte

FZKA 6679

Post-irradiation studies on the (U, Pu)O_2 cluster experiment POUSSIX in the PHENIX reactor

H. Kleykamp

Institut für Materialforschung

Programm Nukleare Sicherheitsforschung

Forschungszentrum Karlsruhe GmbH, Karlsruhe

2001

Als Manuskript gedruckt
Für diesen Bericht behalten wir uns alle Rechte vor

Forschungszentrum Karlsruhe GmbH
Postfach 3640, 76021 Karlsruhe

Mitglied der Hermann von Helmholtz-Gemeinschaft
Deutscher Forschungszentren (HGF)

ISSN 0947-8620

Nachbestrahlungsuntersuchungen am (U, Pu)O_2 Cluster-Experiment POUSSIX im PHENIX-Reaktor

Zusammenfassung

Zwölf Schnellbrüterstäbe mit $U_{0,78}Pu_{0,21}Am_{0,01}O_{1,955}$-Brennstoff wurden als Clusterexperiment im PHENIX-Reaktor bis zu 9,6 % Abbrand bestrahlt. Die hauptsächlichen Versuchsparameter der Stäbe waren die Schmierdichte, die Spaltbreite zwischen Brennstoff und Hülle und die Tablettengeometrie ohne oder mit zentralem Loch. Drei Querschnittsproben wurden ausgewählt für die Röntgenmikrosonden-Untersuchungen der radialen Konzentrationsumverteilung von U, Np, Pu und Am im Brennstoff, des Brennstoffes und der Spaltprodukte im gefüllten Zentralkanal, der metallischen und keramischen Ausscheidungen und der Brennstoff-Hülle-Wechselwirkung. Das O/M-Verhältnis des Brennstoffs bei Bestrahlungsende wurde durch Röntgenbeugung aus der Gitterkonstante ermittelt. Es werden eine starke radiale Umverteilung von Np, Pu und Am in Richtung des Spalts und ein ausgeprägter axialer Brennstofftransport entlang des Zentralkanals zum oberen und unteren Stabende beobachtet. Ein Einfluss der Tablettenparameter auf die Umverteilungsphänomene wurde nicht festgestellt. Das querschnittsgemittelte O/M-Verhältnis bei Bestrahlungsende beträgt 1,95 am oberen Stabende. Hier besteht ein Hüllangriff bis zu etwa 20 µm Reaktionsschichtdicke. Hier wird ferner eine hohe Stableistung vermutet, weil der Zentralkanal und der Spalt vollständig mit Brennstoff bis zu etwa 60 % PuO_2 und überdurchschnittlichen Anteilen an Np und Am gefüllt sind. Die Wärmeleitfähigkeit des Brennstoffs ist niedrig wegen des geringen O/M-Verhältnisses. Beide Effekte können zu einer erhöhten Hüllinnen- und Brennstoffzentraltemperatur am oberen Stabende führen.

Abstract

Twelve fast breeder $U_{0.78}Pu_{0.21}Am_{0.01}O_{1.955}$ fuel pins were irradiated as a cluster experiment in the PHENIX reactor up to 9.6 % burnup. The principal test parameters of the pins were the smear density, the fuel-clad gap width and the solid/annular geometry of the pellets. Three pin cross-sections were selected to study the radial concentrations of U, Np, Pu and Am in the fuel, the fuel and fission product compositions of the filled central void, the metallic and ceramic precipitates, and the fuel-clad interactions by X-ray microanalysis. The end-of-life O/M ratio of the fuel was investigated by X-ray diffraction. A strong radial redistribution of Np, Pu and Am to the gap is marked. There is a pronounced axial fuel transport along the central void to the upper and lower fuel pin ends. An influence of the pellet parameters on the relocation phenomena was not stated. The end-of-life O/M ratio of the upper end fuel region is 1.95. The maximum inner clad corrosion is observed in the hottest upper end clad region with about 20 µm thickness. A high linear heat rating is assumed in this pin region, because the central void and the gap region are completely filled with fuel up to about 60 % PuO_2 and high fractions of Np and Am. The thermal conductivity of the fuel is low due to the reduced O/M fuel ratio. Both effects may increase the inner clad temperature and the fuel centre temperature significantly.

CONTENTS

1. Introduction 1

2. Fuel and pin data 1

3. Irradiation data 1

4. General post-irradiation examination 2

5. Pin cross-sections for X-ray microanalysis 2

6. Actinide distribution 4

7. Dissolved and submicroscopically precipitated fission products 5

8. Metallic precipitates 5

9. Ceramic precipitates 7

10. Compatibility between fuel and cladding 8

11. Discussion and summary 9

12. Conclusion 9

Acknowledgements 10

References 10

Figures 11

1 Introduction

The POUSSIX experiment was outlined as a common CEA/DEBENE fast breeder irradiation in the PHENIX reactor. The method of approach was the optimisation of the smear density of the uranium-plutonium oxide fuels by variation of the pellet type (annular or solid) and the gap size between fuel and cladding as well as the implications on the mechanical behaviour of the pins at high burnups. Twelve fuel pins in the Mark II geometry were irradiated up to 9.6 % burnup corresponding to 85 dpa (NRT). The fuels had been fabricated by Alkem and Belgonncleaire by different routes, e.g., OCOM and AUPUC fabrication with solid and annular pellets. Various cladding materials were used, e.g., austenitic stainless steel 1.4970, 15 % cold worked and aged, and ferritic steel.

The importance of the experiment from the present-day view is the behaviour of the actinides with respect to their build-up, distribution and relocation during the irradiation process. The main issues are the so-called minor actinides, neptunium, americium and curium, which play a major role in the actinide transmutation projects. Therefore, the actinides and long-living fission products and their chemical state are treated with emphasis in this report.

Three austenitic steel cladded pins have been selected for non-destructive and destructive post-irradiation studies at Forschungszentrum Karlsruhe of which the fuel and pin properties and the irradiation behaviour are described in the next sections.

2 Fuel and pin data

The mixed oxide fuel of the selected pins was prepared from UO_2 powder with U-235/U-tot = 0.73 % and PuO_2 powder with Pu-fiss/Pu-tot=75.8 % by the optimised co-grinding method (OCOM). The americium content was reported by 1.21 % of the total actinides (February 1984). The total composition results in $U_{0.779}Pu_{0.209}Am_{0.012}O_{1.956}$. Pellet type, diameter and density, O/M ratio, diametrical gap and smear density are compiled in Table 1. The pin length is 1500 mm, the fuel length 750 mm, outer cladding diameter 7.60 mm, inner cladding diameter 6.60 mm. The cladding material is austenitic steel 1.4970, cold worked and aged (annealed). The pins were filled with 1 bar helium at room temperature.

3 Irradiation data

The assembled twelve wire-spaced pins were irradiated in a cluster in the PHENIX reactor within the period October 1984 to July 1987 corresponding to 587 full power days. The linear heat rating of about 33 kW/m was increased to the maximum value of 45 kW/m not before 200 full power days. The pins with the highest smear density attained the highest linear heat rating.

Samples of three pins have been selected for destructive post-irradiation studies at Forschungszentrum Karlsruhe. The irradiation data of these pins are compiled in Table 1 [1,2].

Table 1: Fabrication and irradiation data of selected pins of the POUSSIX irradiation experiment [1,2].

pin number	1	4	11
French pin designation	7	5	2
fuel fabrication	OCOM	OCOM	OCOM
fuel pellet type	annular	solid	solid
pellet diameter	6.417 mm	6.474 mm	6.325 mm
pellet density	96.5 %	96 %	96 %
diametrical gap	182 µm	124 µm	277 µm
smear density	88 %	93 %	88 %
O/M ratio	1.957	1.955	1.955
max. lin. heat rating	42 kW/m	45 kW/m	42 kW/m
max. mid-wall clad. temp.	620°C	635°C	619°C
max. burnup	8.8 %	8.9 %	8.7 %
fission gas release	65 %	66 %	69 %
length of filled central void after irradiation			
- upper pin end	66 mm	32 mm	40 mm
- lower pin end	7mm	150 mm	18 mm

4 General post-irradiation examination

Betatron radioscopy of pin No. 1 (annular pellets) and of pins No. 4 and 11 (solid pellets) revealed fuel-filled central voids at both the upper and lower pin ends. Abundant axial fuel transport took place toward both directions from the pin region of maximum linear heat rating (see Table 1). This observation is supported by the extraordinary high central void radius up to 0.5 r_o (r_o is the fuel pellet radius). The lowest BOL fuel centre temperature (lowest linear heat rating) was estimated in the upper part of the pin. Therefore, the length of the filled central void section in this region is in general higher than in the lower part of the pin, where the fuel temperature was not as low as in the upper part of the fuel pin.

The relative fuel averaged fission gas release of the pins was evaluated from calculations of the generated fission gas (yield and burnup) and experimental determinations of the free fission gas by pin piercing. The pin-averaged value of the released fraction amounts to about 67 %, see Table 1.

5 Pin cross-sections for X-ray microanalysis

A total of three samples from three different pins were selected for X-ray microanalysis. The cross-sections originate from pin regions with different thermal loads and burnups, resp. The local irradiation data are compiled in Table 2. The samples were thinned and were partly cut in half in order to minimise the plutonium inventory below 0.2 g per unit and to limit the γ-

dose rate to 3 mSv/h in 30 cm distance. The embedding by the usual metallographic techniques took place in the end of 1994. The analyses were performed by use of the shielded X-ray microanalyser Jeol JRXA-50/JSM-6400 in 1995. Emphasis was laid on the quantitative analysis of the minor actinides neptunium, americium and curium. Therefore, the measurements in these sections were repeated in 1997 after careful preparation of improved standards and preceding calculations of detection limits of these elements.

The standards used for the actinide analysis were, uranium: UO_2, neptunium: 2.0 % $^{237}NpO_2$ dissolved in borosilicate glass; plutonium: PuO_2, americium $U_{0.5}Am_{0.5}O_2$; curium: 1.7 % $^{244}CmO_2$ dissolved in borosilicate glass. The measurements were made using the working voltage 15 kV, beam current 140 nA, counting time for step scans and point analysis 200 s. In order to avoid X-ray emission lines interferences, U and Np were analysed using the $M\alpha_1$ lines, Pu, Am and Cm were analysed using the less intense $M\beta$ lines [3,4]. The calculated detection limit for Np is c_{min} = 0.06 %, for Cm is c_{min} = 0.09 %. These figures are comparatively high on account of the high γ-dose rates of the samples in the order of 3mSv/h (300 mrem/h) in 30 cm distance. The minor actinide build-up is given by the following schemes:

^{237}Np build-up

a) $^{238}U(n,2n)^{237}U(\beta)^{237}Np$ (largest portion)

b) $^{241}Am(\alpha)^{237}Np$

c) $^{235}U(n,\gamma)^{236}U(n,\gamma)^{237}U(\beta)^{237}Np$

^{241}Am build-up

$^{241}Pu(\beta)^{241}Am$

^{244}Cm build-up

$^{242}Pu(n,\gamma)^{243}Pu(\beta)^{243}Am(n,\gamma)^{244}Am(\beta)^{244}Cm$

Table 2: Fuel and irradiation data of selected pin cross-sections of the POUSSIX irradiation experiment.

pin number	1	4	11
cross-section (sample) No.	6	3	1
distance from lower fuel end	690 mm	445 mm	390 mm
pin region	$T_{clad,max}$	upper region	χ_{max}
clad mid-wall temp.	615°C	568°C	550°C
calc. burnup	6.2 %	9.1 %	9.5 %
max. lin. heat rating	25 kW/m	38 kW/m	42 kW/m
central void	filled with fuel	filled with met. fission products	void
central void radius	$0.06 \cdot r_o$	$0.18 \cdot r_o$	$0.36 \cdot r_o$
xenon release*	96 %	95 %	99 %
burnup by Nd conc.*	6.9 %	(11.0 %)	9.4 %

* measured by X-ray microanalysis.

The light-optical microstructures and the α- and β-autoradiographs of the cross-sections of samples No. 6 (pin No. 1), No. 3 (pin No. 4) and No. 1 (pin No. 11) are presented in Fig. 1, Fig. 12 and Fig. 19, resp. The positions of detailed analyses are marked in the microstructures. The central void at the upper pin end (annular pellets, sample No. 6, Fig. 1) is nearly completely filled with fuel; the central void toward the upper pin end (solid pellets, sample No. 3, Fig. 12) is filled with a metallic fission product ingot; the largest central void in the pin region of the maximum linear heat rating is empty (solid pellets, sample No. 1, Fig. 19).

6 Actinide distribution

The concentration of the actinides U, Np, Pu and Am (in mass % MO_2) of the three cross-sections are presented as a function of the relative fuel radius r/r_o in Fig. 2, Fig. 13 and Fig. 20.

Cross-section No. 6 of pin No. 1. The central void (ZK) is nearly completely filled with fuel, the concentration of the components is independent of the fuel radius with the exception of the fuel surface and gap regions. Due to the strong initial hypostoichiometry of the fuel, O/M = 1.957, the PuO vapour pressure is high and therefore, radial and axial transport occur from the maximum heat rating region towards the fuel surface and the fuel ends with high Pu, Am and Np contents of 60 % PuO_2, 1.4 % AmO_2 and 0.3 % NpO_2 on the fuel surface (Fig. 2).

The Pu and U distribution images in Fig. 4 and the concentration profiles of Pu (in % PuO_2), Zr, Ce and Nd in Fig. 5 demonstrate a 75 µm thick PuO_2 rich mixed oxide outer layer up to 68 % PuO_2 and a local burnup of about 8 % which was calculated from the concentration of Nd dissolved in the fuel. The same behaviour was observed on the opposite side of the fuel surface region in Fig. 6 with maxima of 46 % PuO_2 and 0.75 % AmO_2. Proportionality exists between Pu and Am with a Pu/Am ratio of about 60 in the fuel surface region.

X-ray diffraction analysis of the total cross-section No. 6 of pin No. 1 gave a lattice parameter a of the mixed-oxide fuel to be $a = (546.5 \pm 0.2)$ pm. Using the formula $a = 547.0 - 7.4 \cdot y + 30 \cdot x - 0.083 \cdot b$ [5], where $y = 0.21$ is the PuO_2 fraction in the fuel, $b = 6.2$ % is the local burnup, the cross-section averaged end-of-life O/M ratio can be calculated yielding $(O/M)_e = 2 - x = 1.95$.

Cross-section No 3. of pin No. 4. The central void is filled with a metallic fission product ingot. A slight Pu, Am and Np enrichment of 21 % PuO_2, 0.63 % AmO_2 and about 0.15 % NpO_2 is observed toward the central void (Fig. 13).

Cross-section No. 1 of pin No. 11. A classic radial Pu concentration profile is stated in the maximum heat rating region with a Pu enrichment of 29 % PuO_2 at the central void, a second Pu maximum up to 34 % PuO_2 in the unrestructured fuel zone and a Pu free region on the fuel surface. This behaviour is typical in strongly hypostoichiometric $(U, Pu)O_{2-x}$ (Fig. 20).

The cross-section averaged concentrations of the analysed actinides are compiled in Table 3. The radial Am concentration profile follows the Pu concentration profile in the three cross-sections. The Pu/Am ratio is about 40 inclusive that of the fuel surface region of cross-section No. 6 of pin No. 1. The radial Np concentration profile is independent of the relative fuel radius. However, an intense axial movement was stated toward the outer fuel direction of the upper fuel pin region. The curium concentration in the fuel could not be measured because the levels are below the detection limit of 0.09 %Cm.

Table 3: Cross-section averaged actinide concentrations (in mass % MO_2) of selected samples of the POUSSIX irradiation experiment.

pin-sample	1-6	4-3	11-1
calculated burnup	6.2 %	9.1 %	9.5 %
UO_2	76.3	74.4	73.9
PuO_2	20.7	18.4	21.2
AmO_2	0.52	0.51	0.53
NpO_2	0.17	0.06	0.07
Σ actinide oxides[a]	97.7	93.4	95.7

[a] The differences to 100 % are fission products dissolved in the fuel matrix.

7 Dissolved and submicroscopically precipitated fission products

The fission products are in part dissolved in the fuel (e.g. Y, Nd, Ce, Sr), are components of ceramic fission product precipitates (e.g. Zr, Ba) or they are implanted into the lattice or pores of the fuel (e.g. Xe). The concentration of selected fission products is plotted as a function of the relative fuel radius r/r_o of three specimens in Fig. 3, Fig. 14 and Fig. 21. The cross-section averaged Nd concentration is used to calculate the local burnup on the basis of the Nd fission yield Y_{Nd} = 0.087 % Nd per % burnup. The cross-section averaged Nd concentration is 0.60 % in sample No. 6, 0.96 % in sample No. 3 and 0.82 % in sample No. 1. The respective burnup values are compiled in Table 2. The cross-section averaged concentration of the bonded Xe is 0.03 % in sample No. 6, 0.05 % in sample No. 3 and 0.01 % in sample No. 1. The respective Xe release rates $R = 1 - Xe_{bonded}/Xe_{generated}$ are also compiled in Table 2. The basis for the determination of R are the calculated local burnup and the Xe fission yield Y_{Xe} = 0.115 % Xe per % burnup. The quantitative Xe analysis was executed by interpolation of the Lα intensities of Sn, Sb, Te, Cs, Ba, La standards which gives a hypothetical Xe standard, and by a following ZAF correction of the Xe Lα signal.

8 Metallic precipitates

Two kinds of metallic precipitates were observed within the fuel of section No. 6 of pin No. 1 in its upper pin region: (1) the classic hexagonal ε-phase containing Mo, Tc, Ru, Rh, Pd and Fe up to the relative fuel radius r/r_o = 0.76 and (2) in the outer fuel region a Pd rich face-centred cubic Pd-Fe-Ru phase, see Fig. 9. The Ru/Mo ratio in the ε-phase is abnormal high and amounts to two and higher. This ratio cannot be explained with the fission yield ratio $Y_{Ru}/Y_{Mo} \approx 1.1$ for ^{239}Pu fission and can be interpreted by strong axial Ru transport to the upper fuel end and by radial Mo and Pd transport to the fuel-clad gap where alloying takes place.

Two kinds of metallic precipitates in the fuel were observed in section No. 3 of pin No. 4 which consist of the fission products Mo, Tc, Ru, Rh and Pd up to $r/r_o = 0.75$ of the relative fuel radius. Both phases have the hexagonal structure according to the Mo-Ru-Rh-Pd phase diagram [6], but they have different compositions, e.g. Mo and Ru are complementary components in the phases, see Fig. 16. The reason for the different composition might be an axial fuel and fission product precipitate transport from other axial levels of the pin. The central void is completely filled with a metallic fission product ingot, see Fig. 17. The matrix consists of the hexagonal Mo-Tc-Ru-Rh-Pd-Fe phase in which are precipitated Pd rich Pd_3(Sn, Sb, Te, Fe) phases. Further precipitates of this kind were observed in radial cracks of the outer fuel region, see Fig. 18. The quantitative composition is compiled in Table. 4.

Table 4: X-ray microanalysis of metallic phases in the central void ingot (phases a to e) and the radial fuel crack (phases f, g), Fig. 17 and 18; cross-section No. 3 of pin No. 4 of the POUSSIX irradiation experiment, concentrations in mass %.

element	line	phases						
		a	b	c	d	e	f	g
Mo	Lα	2.0	0.3	0.1	0.2	33.6	0	0
Tc	Lα	0.1	0.1	0.1	0	9.0	0	0
Ru	Lα	0.3	0.1	0.1	0.1	32.3	1.8	0
Rh	Lα	0.5	0.1	0.1	0	9.8	4.3	3.2
Pd	$L\beta_1$	72.2	75.9	72.7	71.5	13.5	65.7	67.0
Sn	Lα	9.0	15.4	14.2	11.3	0	6.6	10.8
Sb	Lα	1.8	1.5	4.9	6.0	0	1.3	1.2
Te	Lα	1.1	0.6	3.7	5.2	0	1.2	1.1
U	Mβ	0.9	0.9	0.8	0.8	0	0	0
Fe	Kα	12.2	5.2	3.3	4.8	1.8	18.9	16.6
Ni	Kα	0	0	0	0	0	0.2	0.2

The composition of the metallic Mo-Tc-Ru-Rh-Pd precipitates in the maximum heat rating region of the mixed oxide matrix is illustrated as a function of the relative fuel radius up to $r/r_o = 0.9$ in Fig. 24. Selected microstructures of the precipitates are illustrated in Fig. 25. Again, the Mo and Pd fractions are low due to their radial gas phase transport to the fuel surface and to the fuel-clad gap where they recondensate together with minor amounts of Sn, Sb, Te and U as well as with cladding components, see Figs. 26 and 27. The quantitative analysis of the precipitates is compiled in Table 5. The compositions indicate a low fuel stoichiometry $(O/M)_e < 1.95$.

The ingot formation of the metallic fission product precipitates is an indicator of the very high fuel temperatures resulting in a radial and axial fuel transport. The refractory metal inclusions Mo, Tc, Ru and Rh are less mobile and coalesce to ingots.

Table 5: X-ray microanalysis of metallic phases near the central void (a to d, Fig. 25) and near the fuel surface (e to h, Fig. 26 and i, Fig. 27) as a function of the relative fuel radius r/r_o; cross-section No. 1 of pin No. 11 of the POUSSIX irradiation experiment, concentrations in mass %.

position	r/r_o	element											
		Mo	Tc	Ru	Rh	Pd	Fe	Ni	Cr	Sn	Sb	Te	U
a	0.38	16.8	12.7	58.3	4.9	6.8	0.05	0.02	0.05	0.07	0.07	0.06	0.3
b	0.39	22.7	12.3	54.5	4.1	6.3	0.06	0.01	0	0	0	0	0.1
c	0.41	14.9	13.7	59.0	5.0	7.0	0.06	0.18	0	0	0	0	0.3
d	0.46	15.6	13.1	59.1	5.0	7.0	0.04	0.13	0	0	0	0	0
i	0.88	10.8	8.1	12.3	67.3	0.8	0.3	0.1	0	0	0	0	0.3
e	0.92	1.8	0.1	0	0.1	63.1	29.6	0.5	1.4	1.8	0.6	0.5	0.6
f	0.94	1.5	0.1	0	0.1	64.6	28.3	0.5	1.2	1.8	0.5	0.5	0.8
g	0.95	1.1	0.2	0	0.2	63.9	29.8	0.4	1.2	1.8	0.5	0.5	0.5
h	0.99	14.4	0	0	0	81.2	0.7	0.2	0.2	0	0.2	0.3	2.8

9 Ceramic precipitates

A family of ceramic precipitates in the fuel was observed in the outer unrestructured fuel zone. The dark grey phases in Fig. 10 and the element distribution images in Fig. 11 point to perovskite phases of the composition ABO_3 with the main components Ba on A sites and Zr, U, Pu on B sites. Cs forms mainly separate phases with U and in lower fractions with Pu in the interface between the fuel and the fission product precipitates. Perovskite phases were quantitatively analysed in the outer fuel region of the cross-section No. 3 of pin No. 4, see Fig. 18. The results are compiled in Table 6. The composition is $(Ba_{1-x-y}Sr_xCs_y)\cdot(U, Pu, Zr, RE, Mo)O_3$. The sum of 100 % mass concentration was not attained because most of the rare earths RE were not analysed that has an influence on the normalised atomic concentrations given in Table 6.

Table 6: X-ray microanalysis of ceramic phase h, i, j, k in a radial fuel crack (Fig. 18); cross-section No. 3 of pin No. 4 of the POUSSIX irradiation experiment, concentration in normalised atom-%.

element	line	phases			
		h	i	j	k
Ba	$L\alpha$	11.6	11.5	11.5	11.8
Sr	$L\alpha$	0.3	0.3	0.3	0.3
Cs	$L\beta_1$	6.3	6.2	6.8	7.2
U	$M\beta$	11.3	11.2	12.2	12.3
Pu	$M\alpha$	2.4	2.4	2.1	2.2
Zr	$L\alpha$	2.3	2.0	1.1	0.8
Nd	$L\alpha$	0.1	0.1	0.1	0.1
Mo	$L\alpha$	0.12	0.35	0.27	0.27
O	$K\alpha$	65.6	66.0	65.6	65.0

Similar results were obtained on the cross-section No. 1 of pin No. 11, see the microstructures in Figs. 22, 26 and 27. The perovskite phases $BaUO_3$ and $BaZrO_3$ and another multi-component Cs-Ba-Mo-Te oxide phase were observed. The quantitative analysis is compiled in Table 7.

Table 7: X-ray microanalysis of ceramic phases near the fuel surface (position 1, Fig. 26; position 2 and 3, Fig. 27; position 4, Fig. 22); cross-section No. 1 of pin No. 11 of the POUSSIX irradiation experiment, concentrations in normalised atom-%.

element	X-ray line	position			
		1	2	3	4
Ba	Lα	3.8	18.9	18.0	18.7
Sr	Lα	0.4	0.4	0.3	0.4
Cs	$L\beta_1$	6.6	1.8	0.6	1.7
U	Mβ	3.5	6.9	14.9	1.5
Pu	Mα	0.1	1.9	1.7	0.8
Zr	Lα	0	8.1	2.1	17.7
Ce	Lα	0	0.1	0.3	0.3
Nd	Lα	0	0.3	0.4	0.2
Mo	Lα	12.5	0.3	0.2	0.4
Fe	Kα	0.9	0.2	0.1	0.1
Sb	Lα	0.1	0	0	0
Te	Lα	9.0	0	0	0
O	Kα	63	61	61	58

10 Compatibility between fuel and cladding

Sample No. 6 of pin No. 1 is located about 60 mm below the upper fuel end with a clad-midwall temperature of 615 °C. The light-optical and electron-optical microstructures as well as the element distribution images are illustrated in fig. 7. The total fuel-clad interaction zone amounts to 120 µm. The thickness of the attacked clad is 20 µm and consists of a steel-Mo-Pd layer. Grain boundary attack was not observed. The 100 µm thick gap is filled with Cs-Ba-Mo oxytelluride and Cs uranate phases. Pu is absent and is enriched on the unaffected fuel surface. The sequence of the stratified phases is illustrated by the concentration profiles of the respective elements in Fig. 8.

The fuel-fission product-cladding reaction behaviour in sample No. 3 of pin No. 4 is characterised by a flaked-off cladding layer which is alloyed with altogether 60 % Mo and Pd and fills the fuel-clad gap together with Cs-Ba oxytelluride and Cs molybdate phases, see Fig. 15. The clad with a midwall temperature of 568°C does not show any intergranular corrosion behaviour.

No clad corrosion was observed in cross-section No. 1 of pin No. 11 with a clad midwall temperature of 550°C, see Fig. 22. The inner clad surface is partly covered with a metallic Pd rich Pd-U-Mo-Fe layer. Concentration profiles across the clad-fuel gap are illustrated in Fig. 23.

11 Discussion and summary

Betatron radioscopy, ceramography, X-ray microanalysis and X-ray diffraction have shown that the fuel is subject to a strong axial and radial material relocation process during irradiation. The bulk density of the fuel and of the material condensed in the central void and in the fuel-cladding gap attained nearly 100 % th. d. in the upper pin region. High enrichments of (Np, Pu, Am)O_2 in the fuel-clad gap of the upper end were observed. The cross-section averaged end-of-life fuel stoichiometry is O/M = 1.95 in this region and even less than O/M = 1.95 in the maximum heat rating region which leads to a strong reduction of the thermal conductivity, a higher linear thermal expansion of the (U, Pu, Am)O_{2-x} fuel and an increase of the fuel temperature. The mechanical fuel-clad interactions may be intensified by these effects. However, the chemical fuel-clad interactions remain unaffected due to the low fuel stoichiometry.

The radial profiles of the Am and Np concentrations are parallel to that of Pu with the exception of the filled fuel-clad gap in the upper pin region where those are a factor three higher than in the fuel. The total Am concentration in the fuel was 1.21 % referred to the total actinides measured in 1984 before irradiation. A cross-section averaged concentration of 0.46 % Am (0.54 % AmO_2) was measured in 1997 after irradiation. The total Np concentration after irradiation was determined to 0.09 % (0.10 % NpO_2) after irradiation. The Cm concentration is below the detection limit of 0.09 %.

12 Conclusion

Strong relocations of the more volatile fuel components take place in the radial direction to the fuel-clad gap and in the axial direction to the upper and lower ends of the central void of fuels with low O/(U+Pu) stoichiometries less than 1.96. The radial transport of Pu in the direction of the fuel-clad gap is a well known phenomenon. A preferred axial transport of Np and Am with high fission cross sections to the upper (and possibly to the lower) fuel pin end was stated in the present analysis. Previous thermal analyses have predicted rather low fuel temperatures at the pin ends. Second thermal and thermomechanical analyses would be necessary in the light of new experimental results of the very low fuel stoichiometry and increased Np, Pu and Am concentrations in the upper pin end region.

Acknowledgement

The author of the present report acknowledges very much the efforts of Messrs. E. Kaiser, G. Weih and F. Weiser from the Metallography Group of the Hot Cells for the specimen preparations and of Mr. H. D. Gottschalg of the Institute of Materials Research I for his careful X-ray microanalysis work.

References

[1] O. Götzmann, POUSSIX CEA/DeBeNe Irradiation Experiment in PHENIX; KfK-5419 (1994)

[2] H. Steiner, M. Heck, Real Case Calculations for POUSSIX Pins with the Fuel Pin Code TRANSIENT, PSF report 3214 (1995)

[3] H. Kleykamp, Z. Naturforschung 36a (1981) 1388

[4] H. Kleykamp, Z. Naturforschung 47a (1992) 460

[5] H. Kleykamp, R. Pejsa, J. Nucl. Mater. 124 (1984) 56

[6] J. O. A. Paschoal, H. Kleykamp, F. Thümmler, Z. Metallkunde 74 (1983) 652

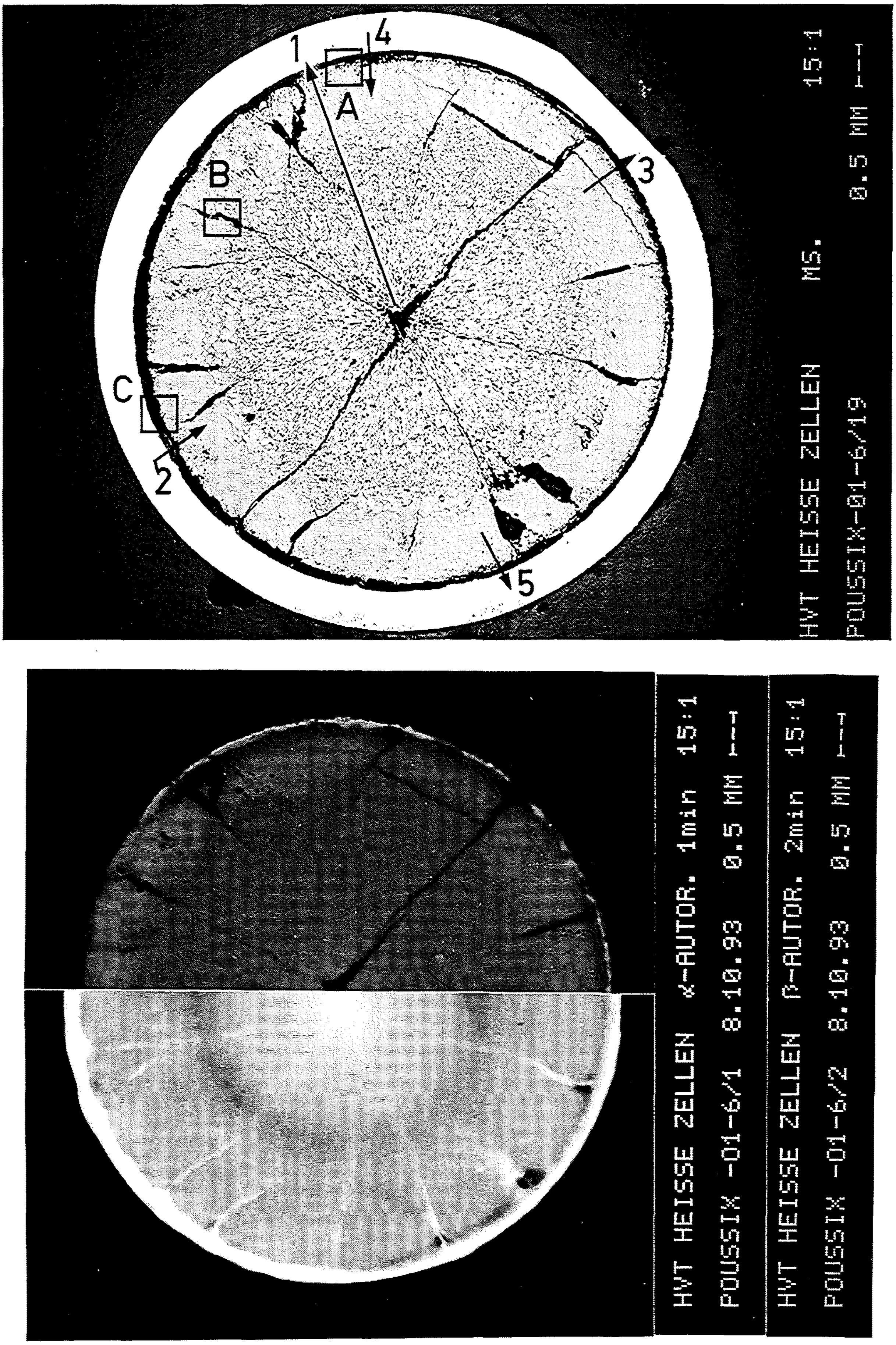

Fig. 1: Microstructure and α- and β-autoradiograph of cross-section No. 6, pin No. 1 of the POUSSIX irradiation experiment. Numbers and letters indicate the positions of detailed analyses in Figs. 2 to 11.

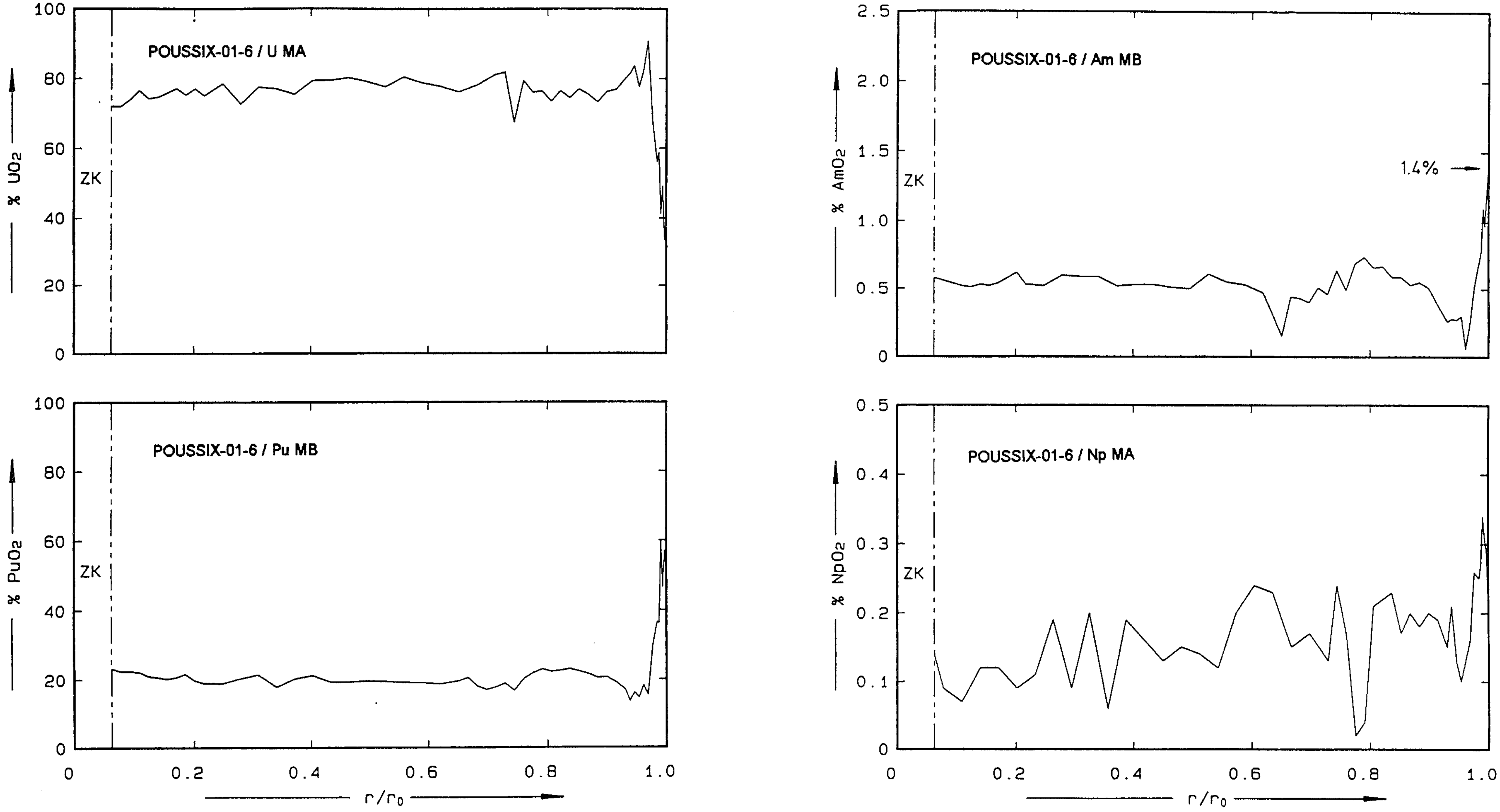

Fig. 2: Radial concentrations of U, Pu, Am and Np (in % MO_2) as a function of the relative fuel radius r/r_o; the central void ZK is on the left side; position 1 in Fig. 1.

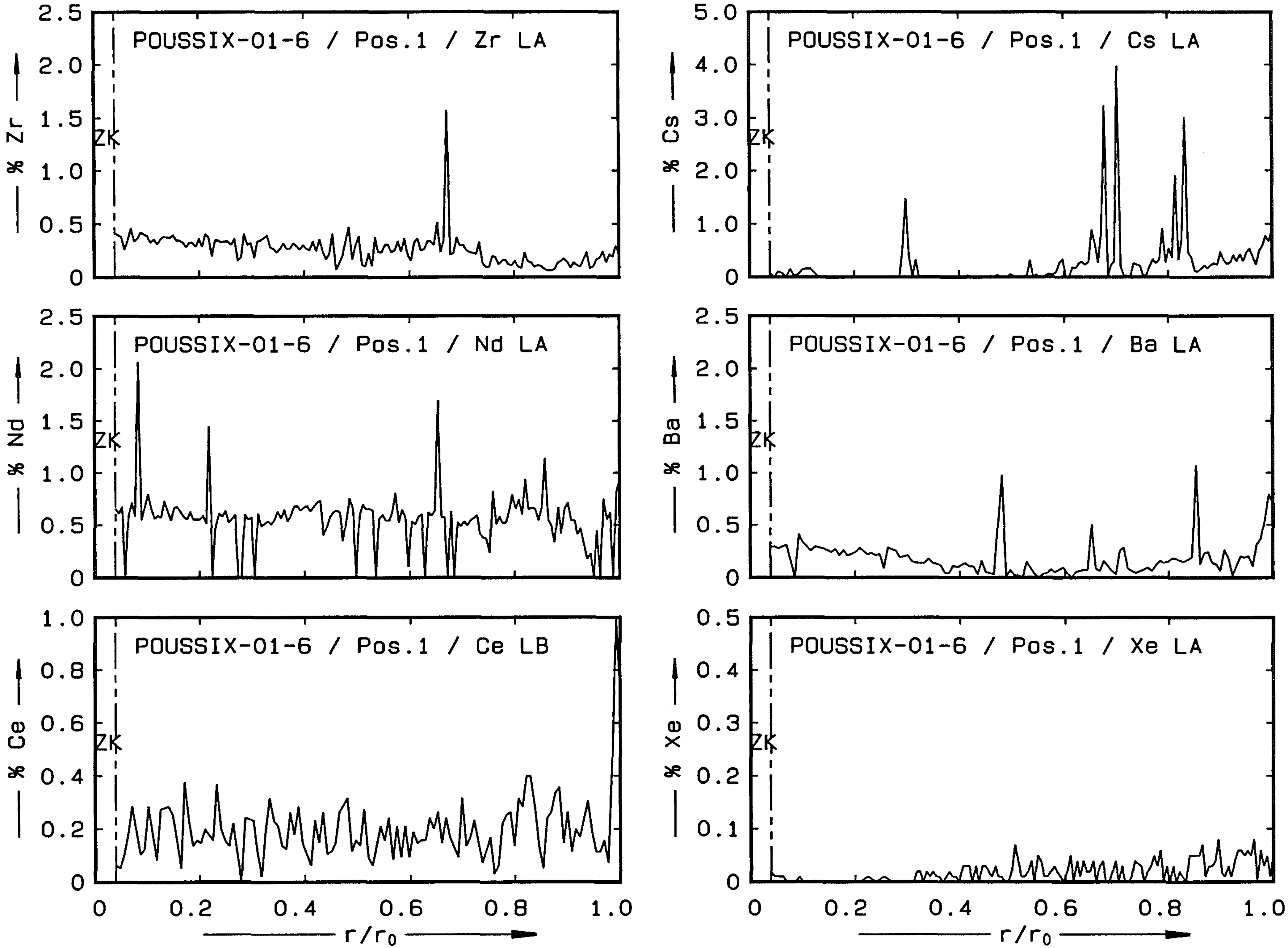

Fig. 3: Radial concentrations of Zr, Nd, Ce, Cs, Ba and Xe as a function of the relative fuel radius r/r_o; the central void ZK is on the left side; position 1 in Fig. 1.

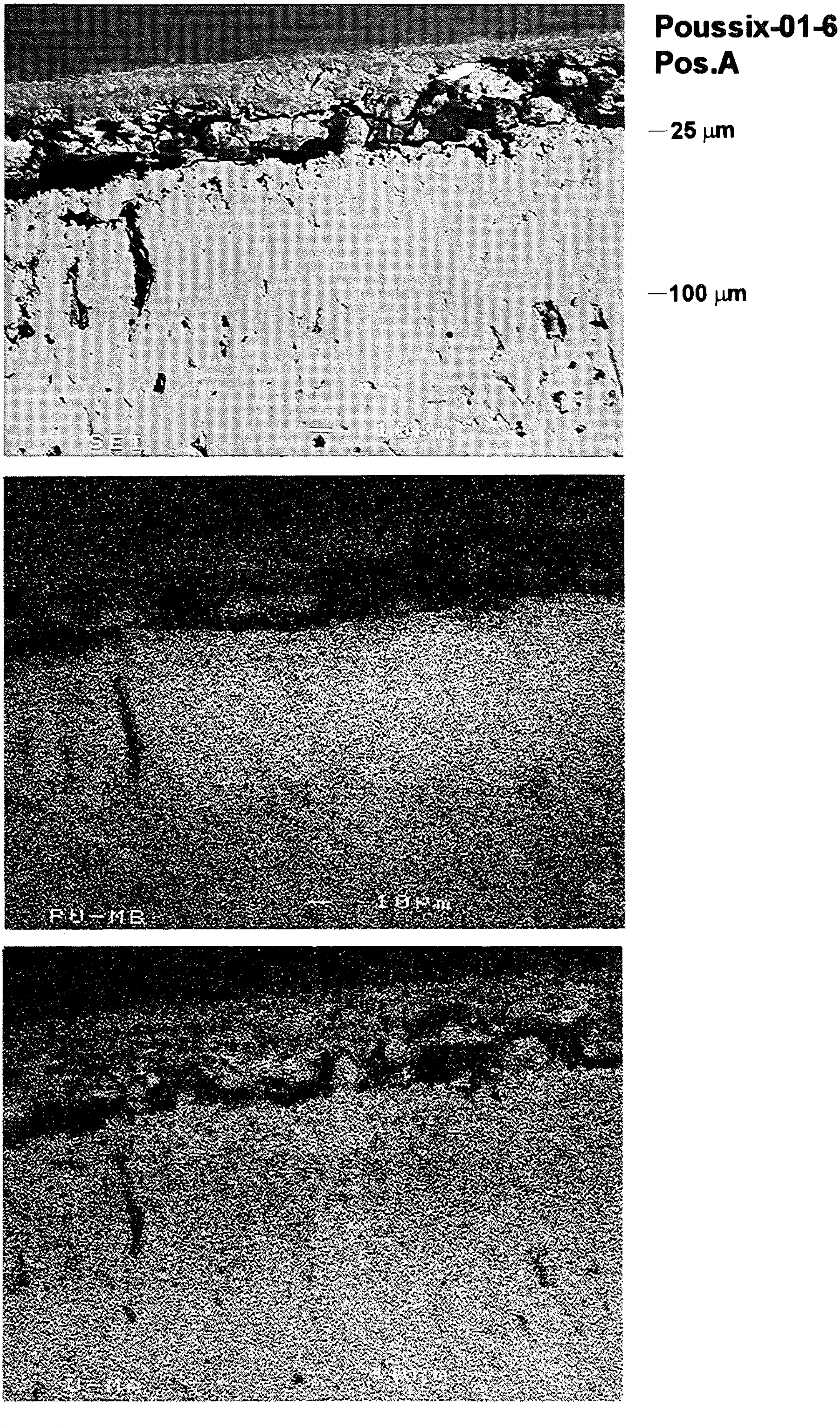

Fig. 4: Secondary electron image and element distribution images of U and Pu (up to 60 % PuO_2) in the outer fuel rim; position A near position 4 in Fig. 1.

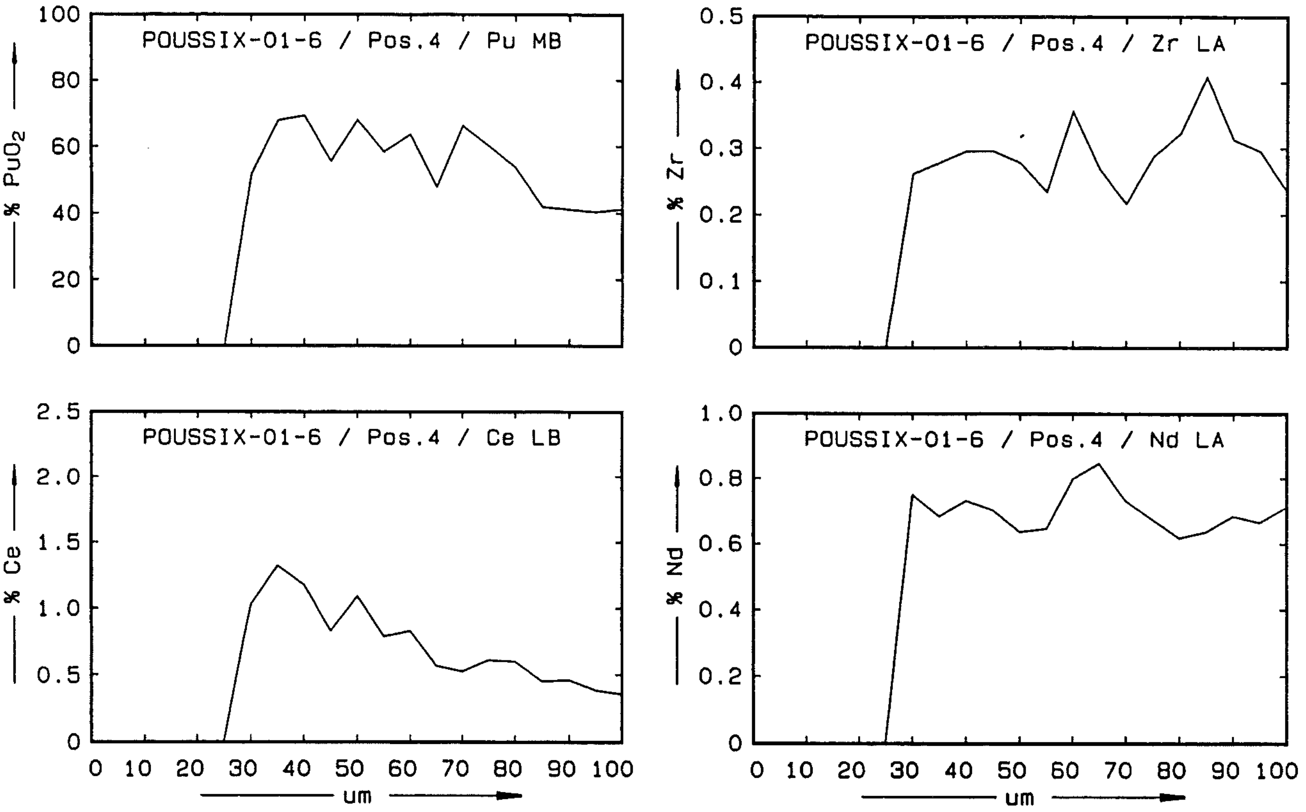

Fig. 5: Concentrations of Pu, Ce, Zr and Nd across the outer fuel rim; position 4 in Fig. 1.

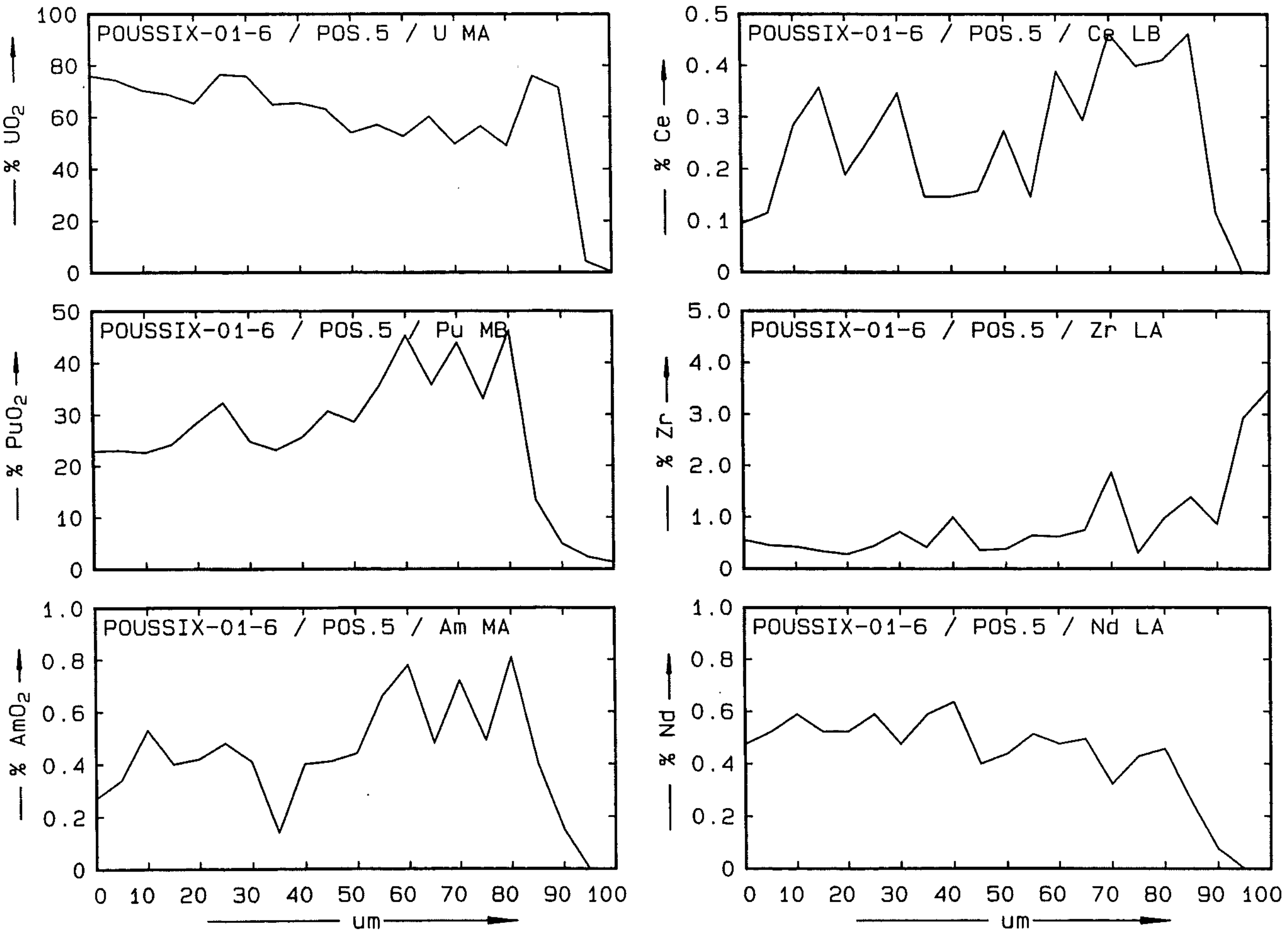

Fig. 6: Concentrations of U, Pu, Am, Ce, Zr and Nd across the outer fuel rim; position 5 in Fig. 1.

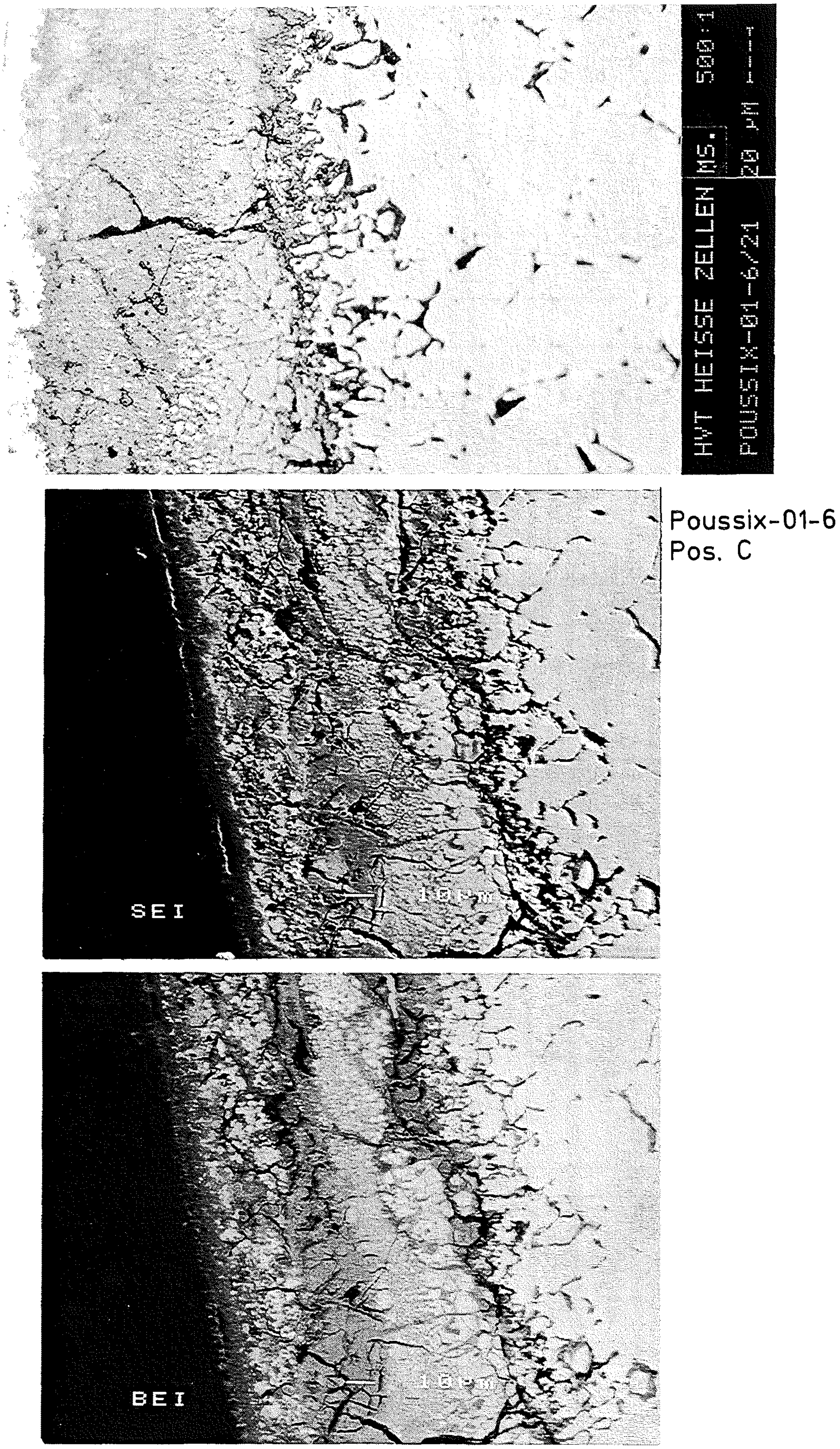

Fig. 7: Light-optical microstructure, secondary and backscattered electron images and element distribution images of Pu, U, Cs, Ba, Te, Cr, Mo, Pd and Fe in the fuel-cladding gap; position C near position 2 in Fig. 1.

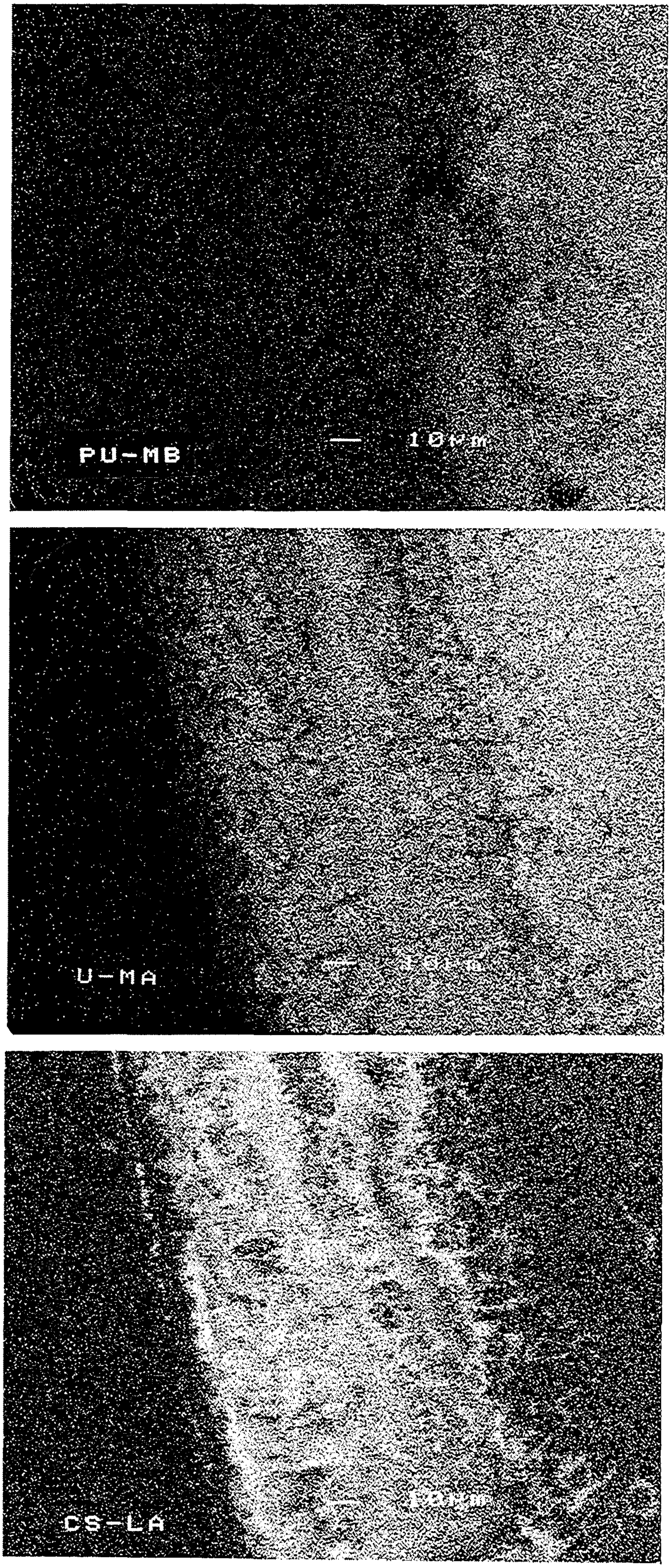

Poussix-01-6
Pos. C

Fig. 7: Continued.

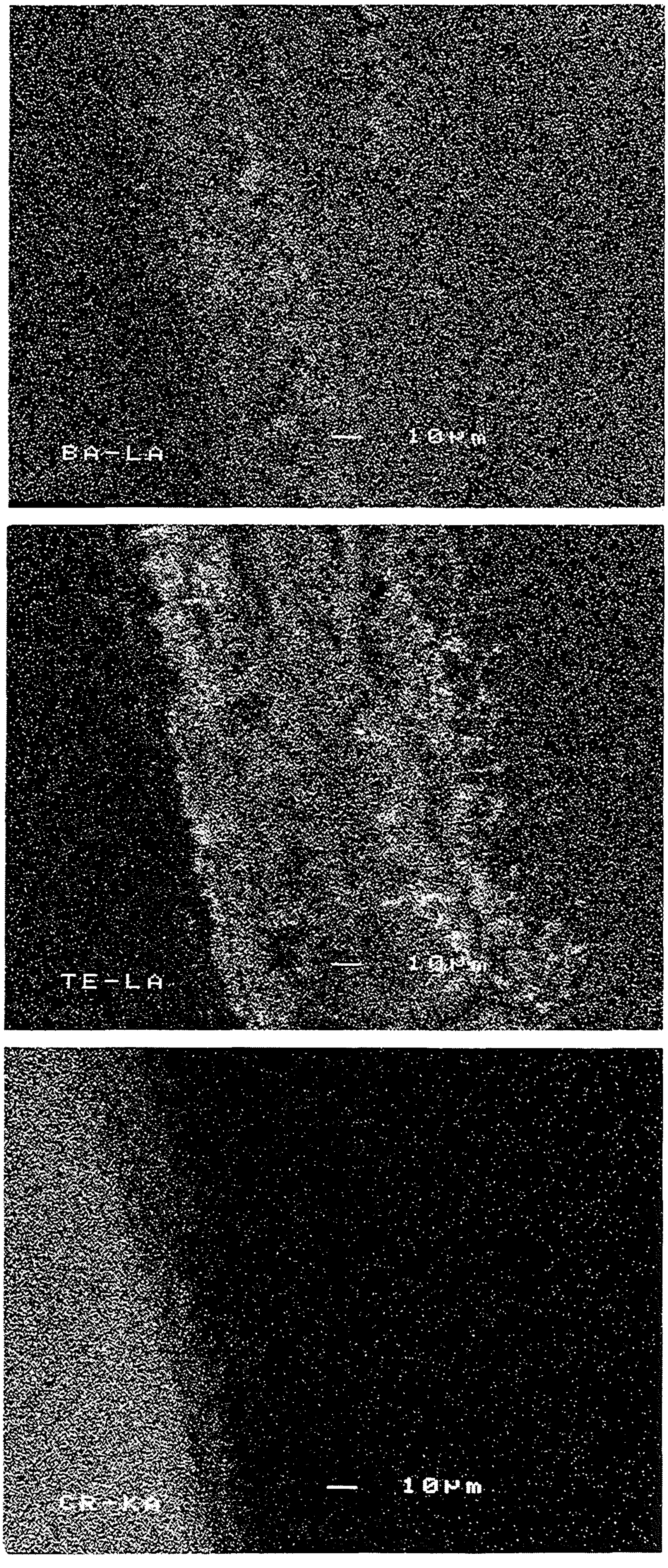

Poussix-01-6
Pos. C

Fig. 7: Continued.

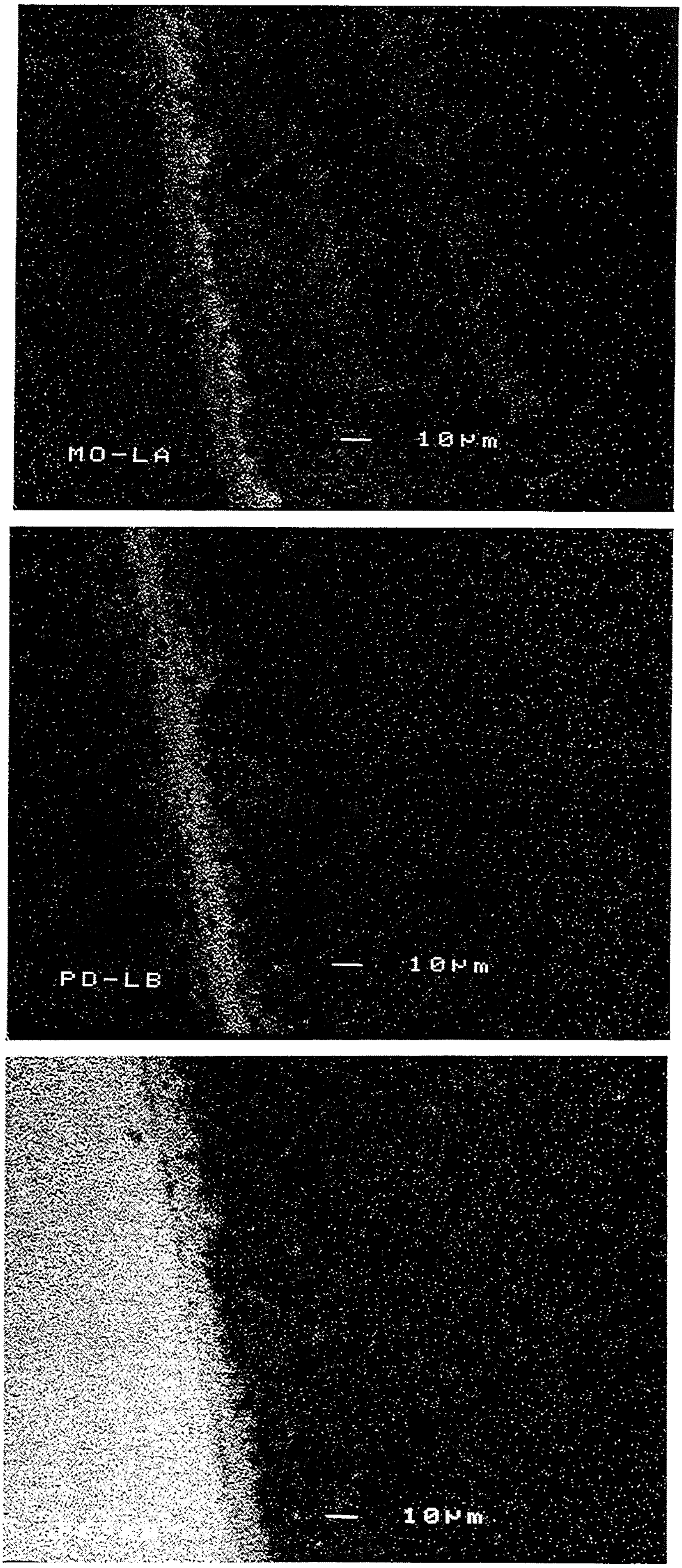

Poussix-01-6
Pos. C

Fig. 7: Continued.

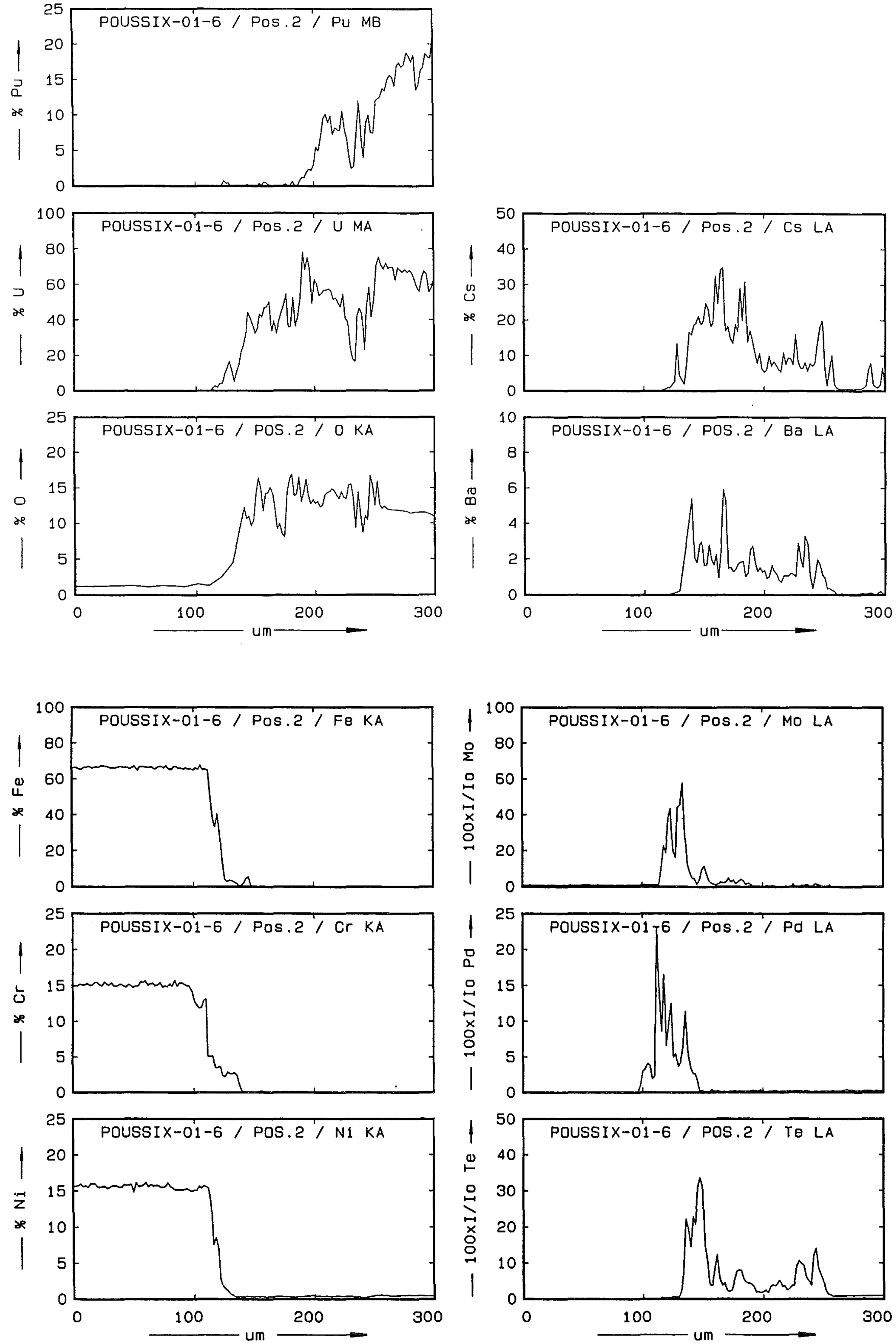

Fig. 8: Concentrations of Pu, U, O, Cs, Ba, Fe, Cr, Ni, Mo, Pd and Te across the fuel-cladding gap; position 2 in Fig. 1.

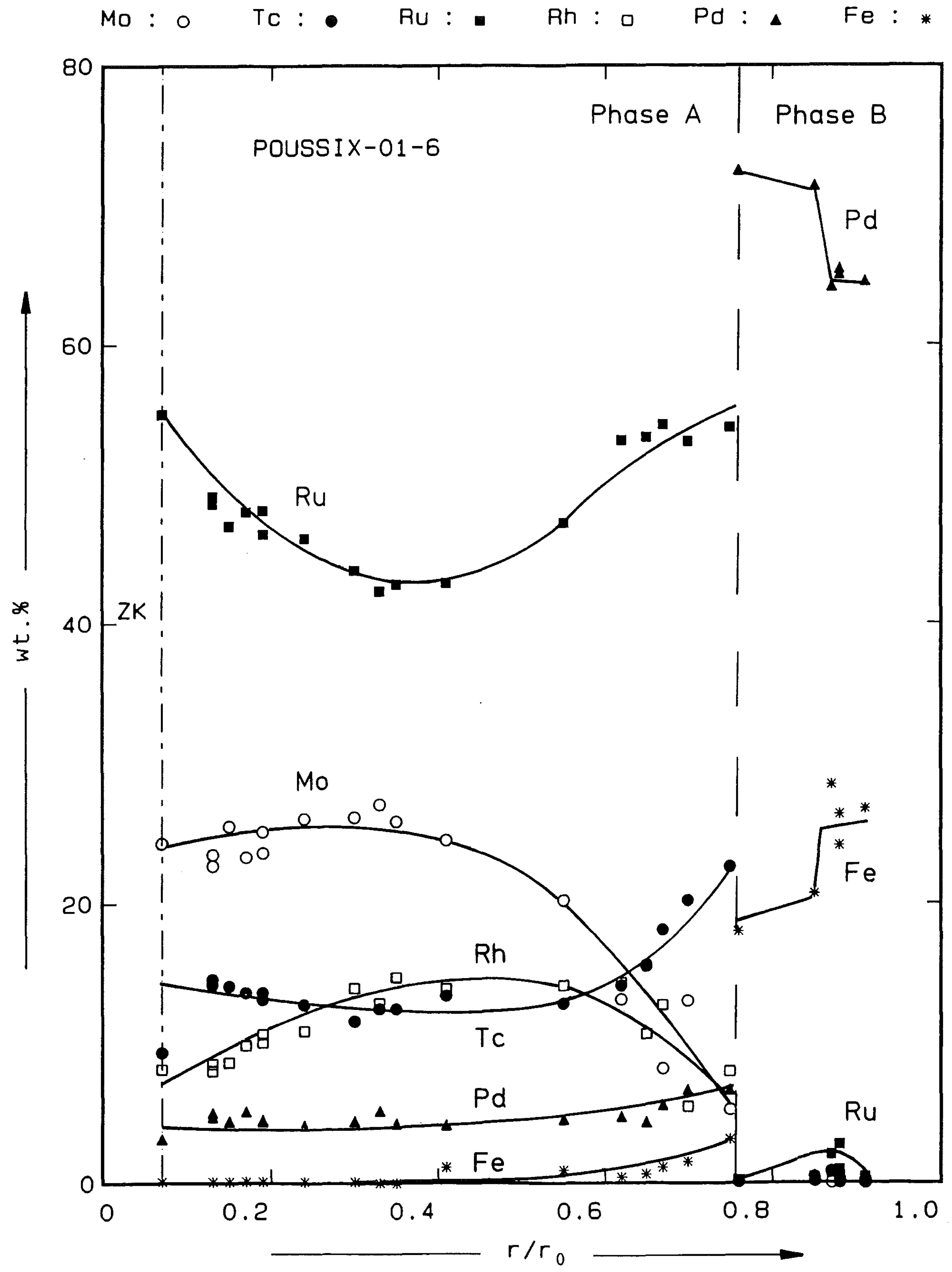

Fig. 9: Composition of the metallic inclusions as a function of the relative fuel radius r/r_0; phase A: hcp. ε-Ru(Tc, Mo, Rh, Pd), phase B: fcc. α-Pd (Fe, Ru).

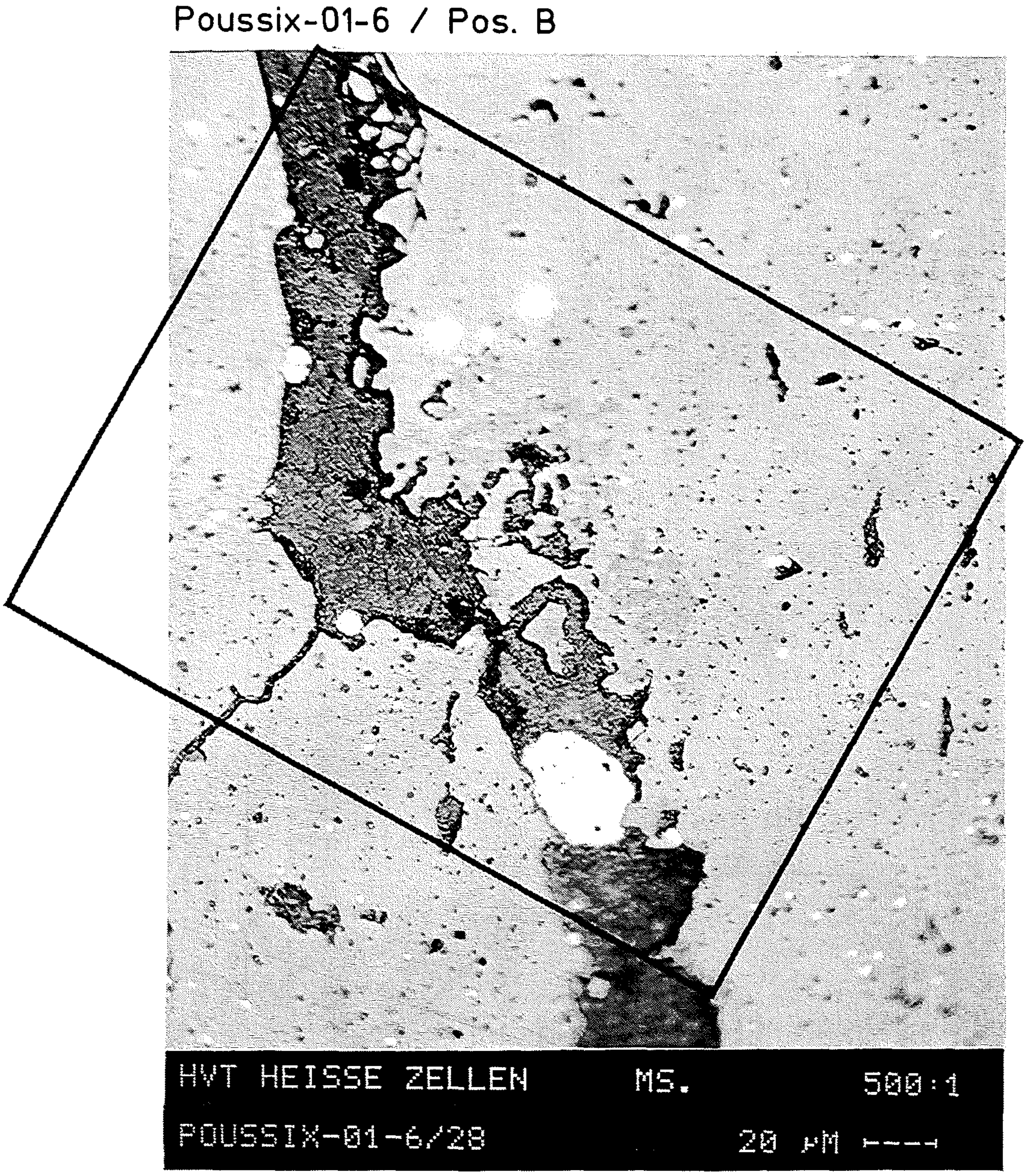

Fig. 10: Light-optical microstructure of metallic and ceramic precipitates at $r/r_o = 0.8$ of the relative fuel radius: α-Pd(Fe, Ru) and $Ba(Zr, U, Pu)O_3$; position B in Fig. 1.

Poussix-01-6 / Pos. B

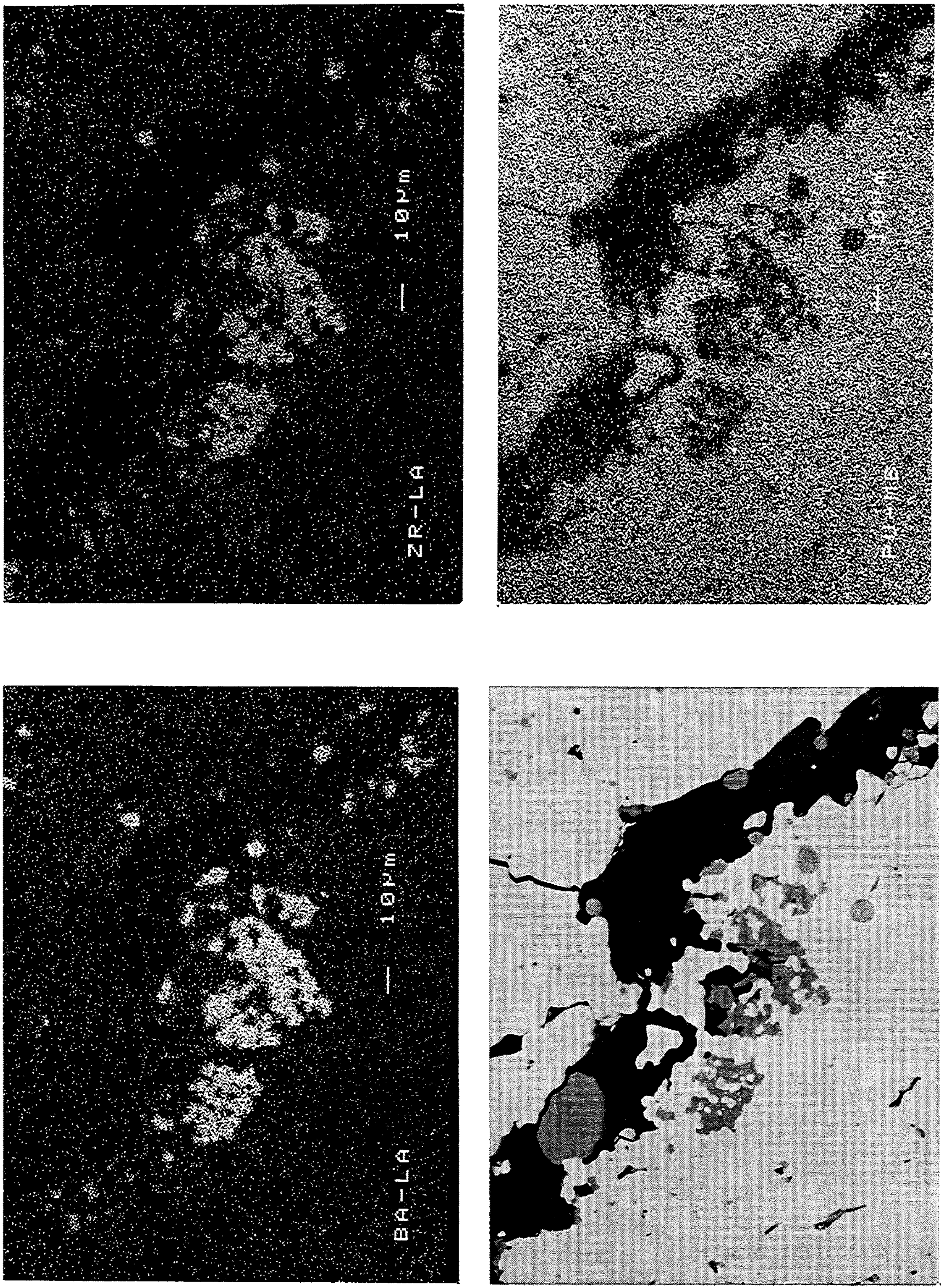

Fig. 11: Backscattered electron image and element distribution images of Ba, Zr, Pu, Pd, Fe, Ru, Cs in the area of Fig. 10; position B in Fig. 1.

Poussix-01-6 / Pos. B

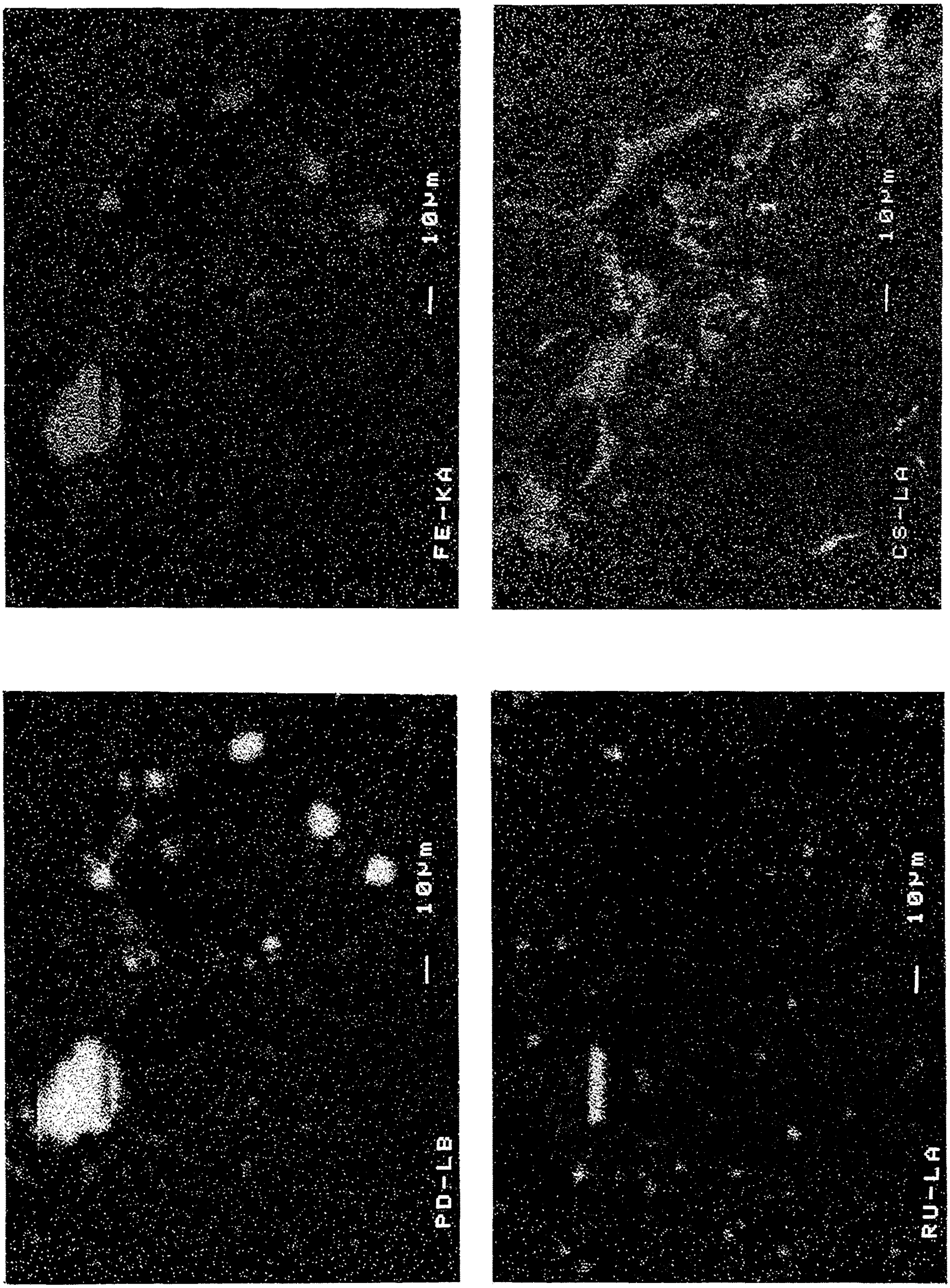

Fig. 11: Continued.

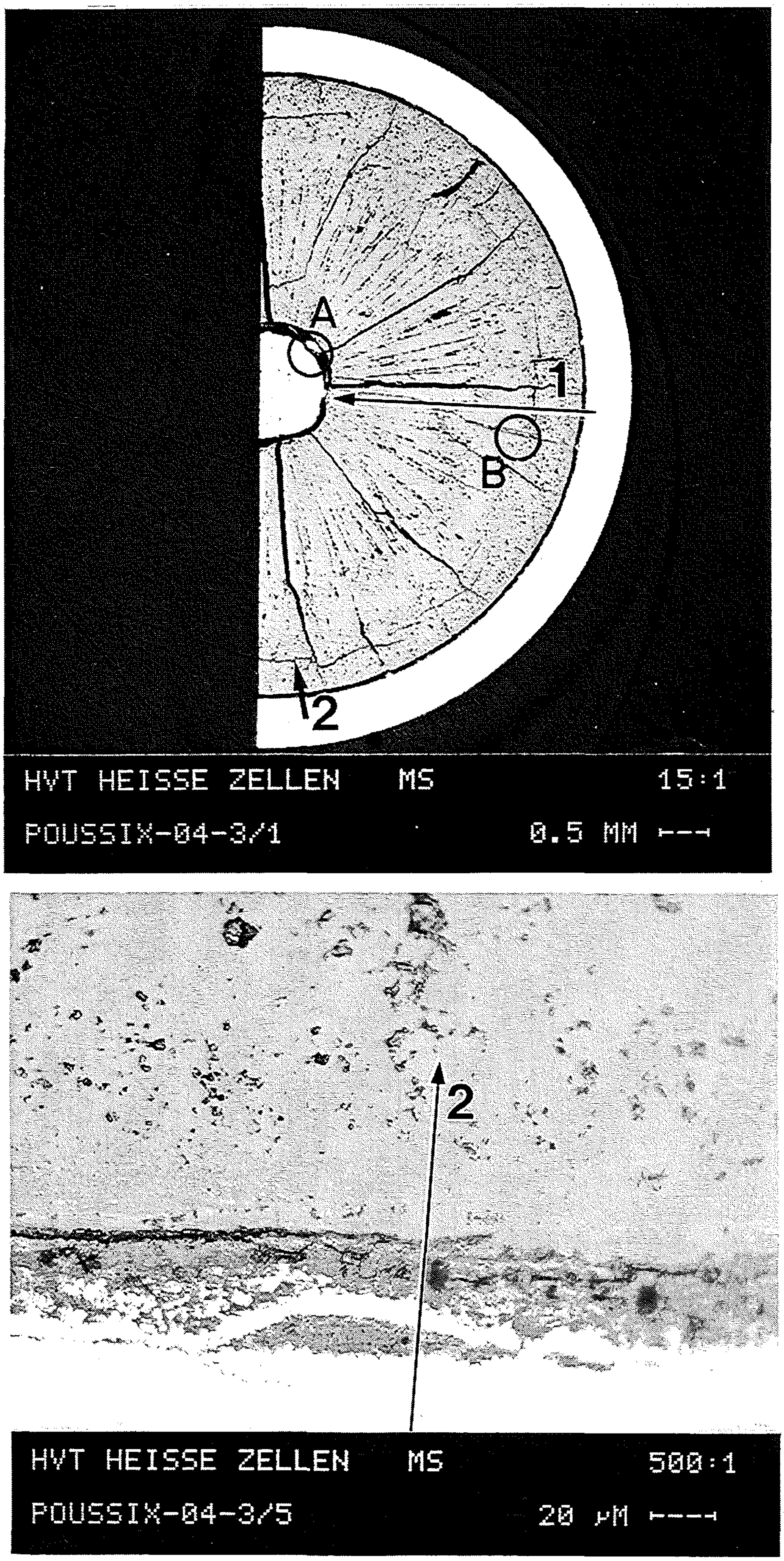

Fig. 12: Microstructure of the half cross-section No. 3, pin No. 4 of the POUSSIX irradiation experiment. Numbers and letters indicate the positions of detailed analyses in Figs. 13 to 18. The lower microstructure in the gap region denotes the track of the concentration profiles in Fig. 15.

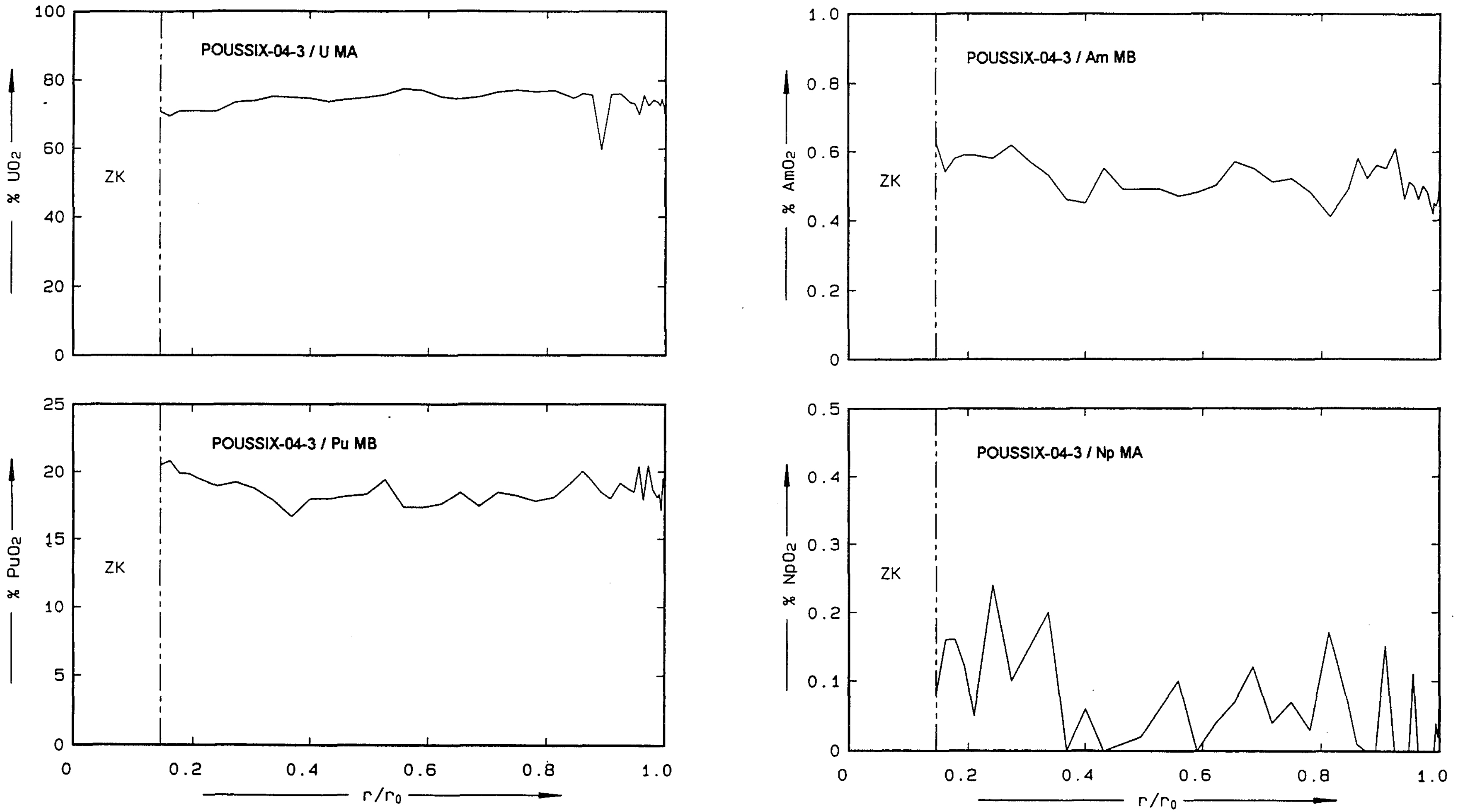

Fig. 13: Radial concentrations of U, Pu, Am and Np (in % MO_2) as a function of the relative fuel radius r/r_0; the central void ZK is on the left side; position 1 in Fig. 12.

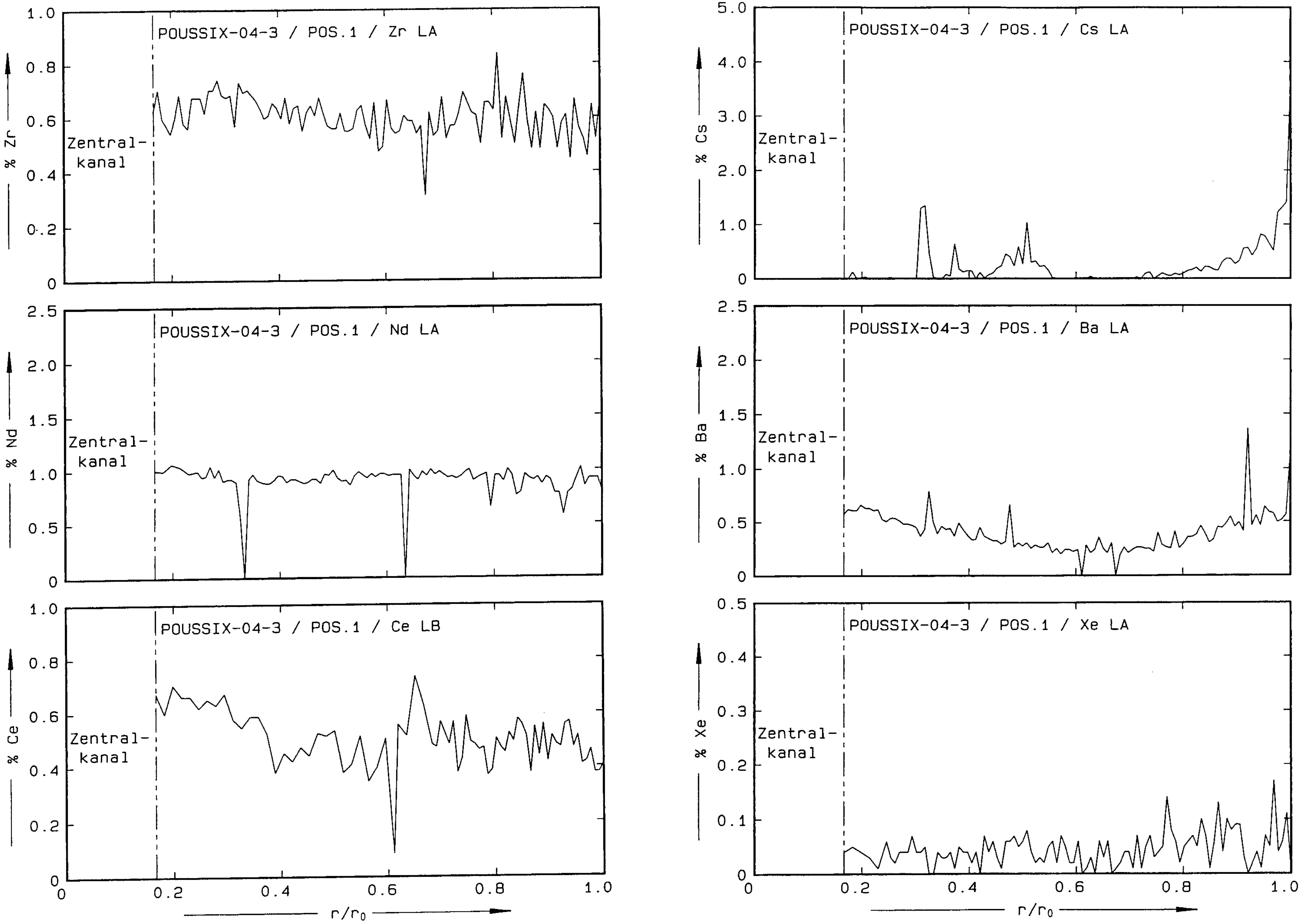

Fig. 14: Radial concentrations of Zr, Nd, Ce, Cs, Ba and Xe as a function of the relative fuel radius r/r_o; the central void ZK is on the left side; position 1 in Fig. 12.

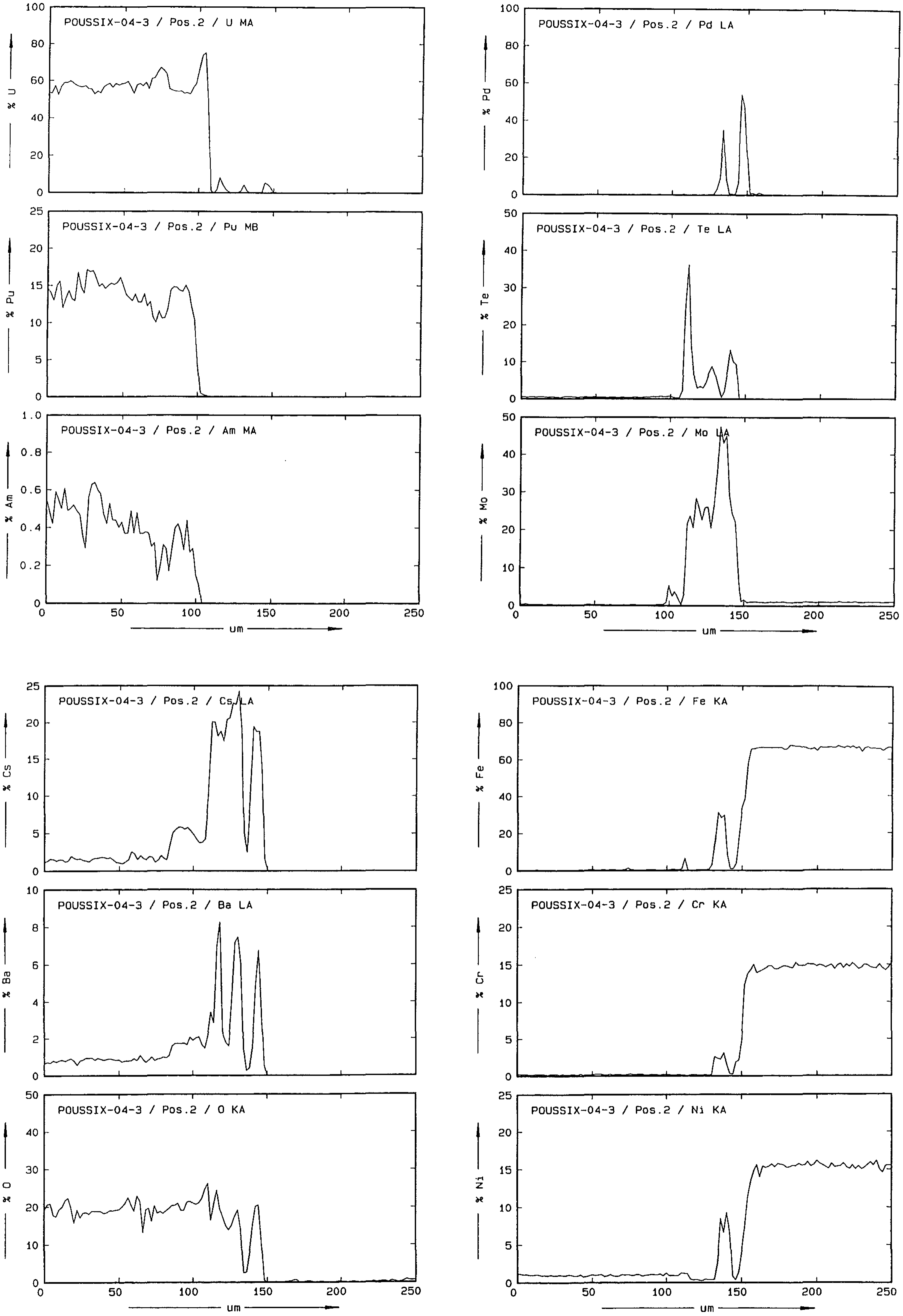

Fig. 15: Concentrations of U, Pu, Am, Cs, Ba, O, Pd, Te, Mo, Fe, Cr and Ni across the fuel-clad gap; position 2 in Fig. 12.

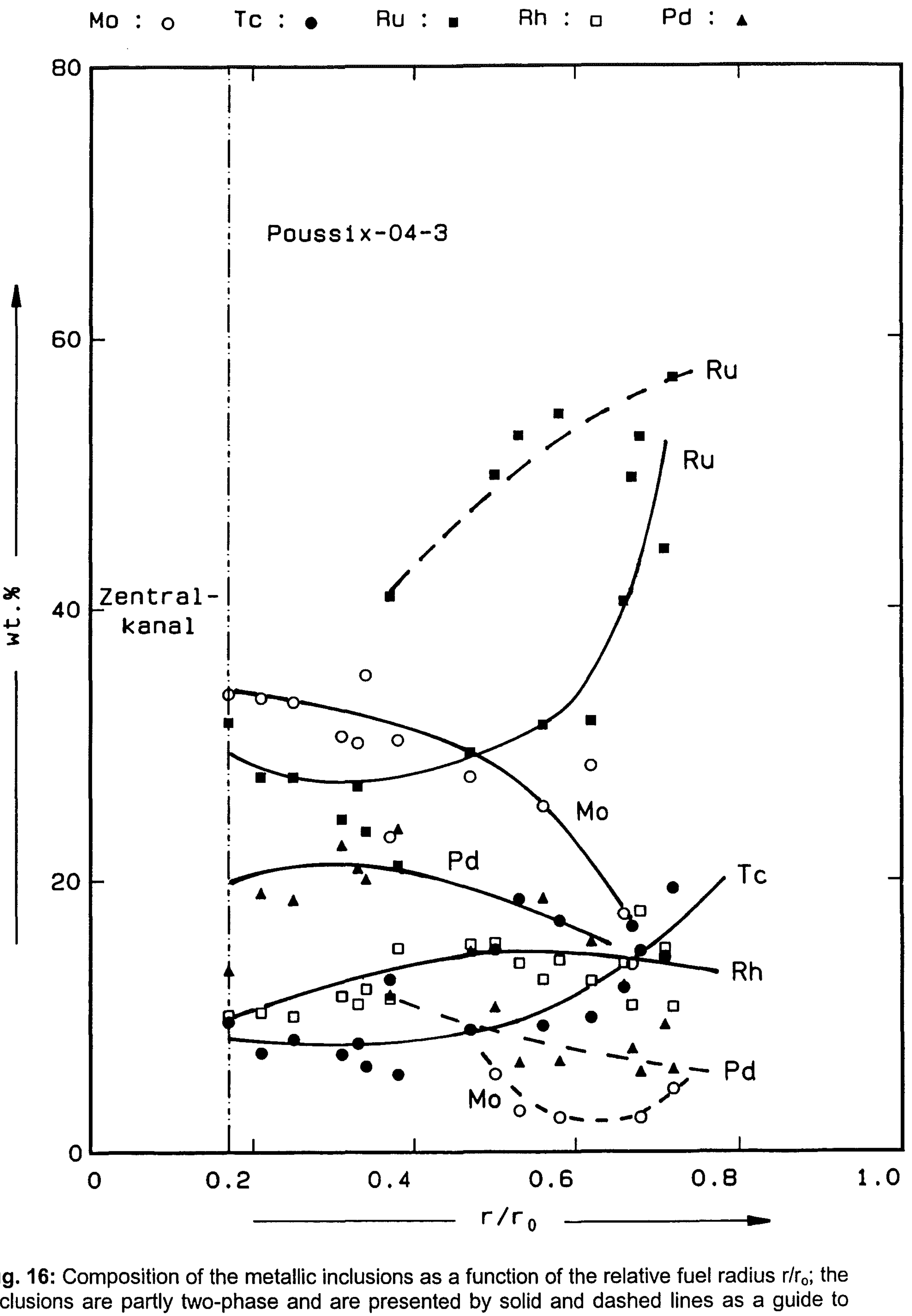

Fig. 16: Composition of the metallic inclusions as a function of the relative fuel radius r/r$_0$; the inclusions are partly two-phase and are presented by solid and dashed lines as a guide to the eye; the fission product filled central void ZK is on the left side.

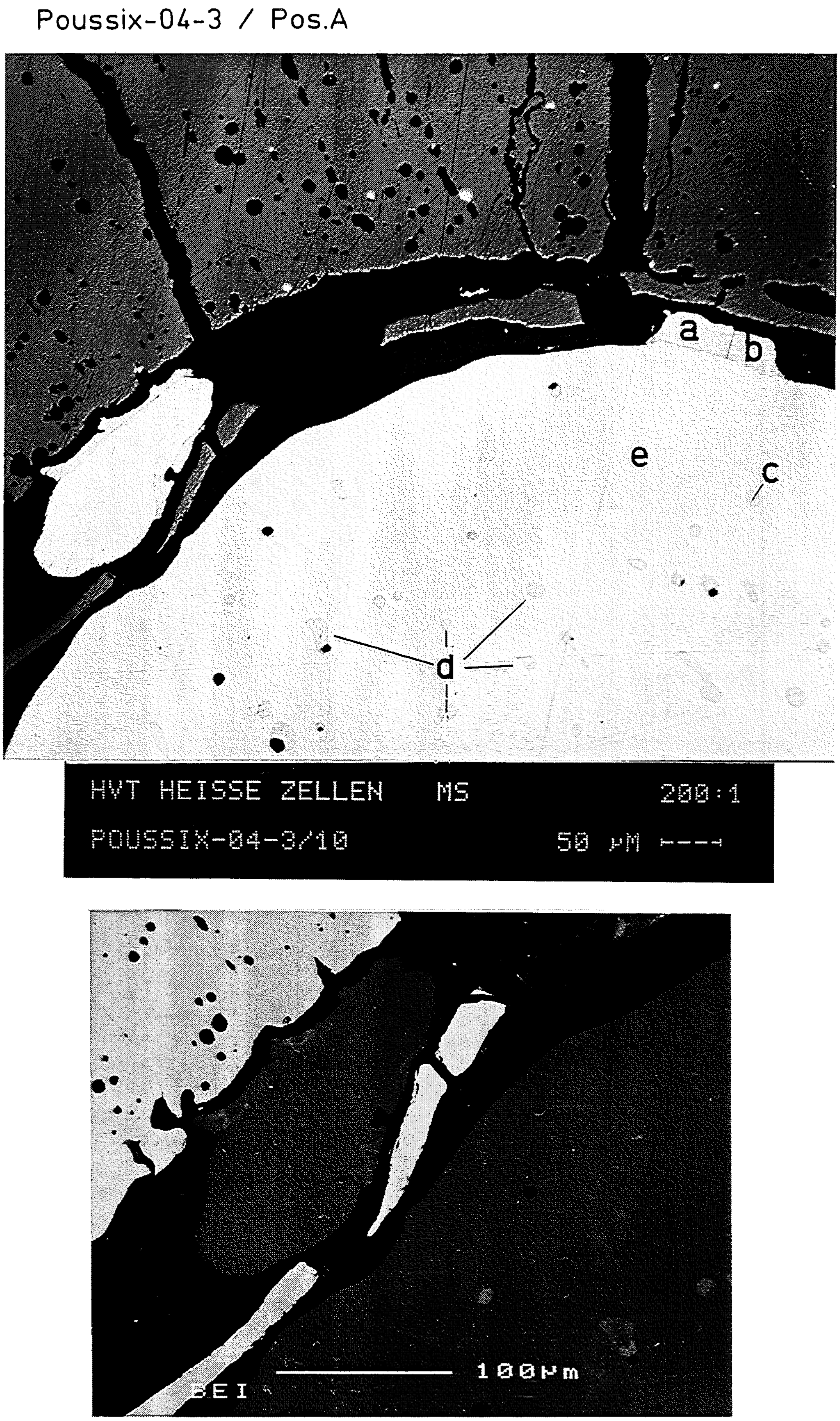

Fig. 17: Light-optical microstructure, backscattered electron image and selected element distribution images of phases in the metallic ingot of the central void: α-Pd(Fe, Sn, Mo, Sb) precipitates are dispersed in an ε-Ru(Tc, Mo, Rh, Pd) matrix, position A in Fig. 12, see also Table 4.

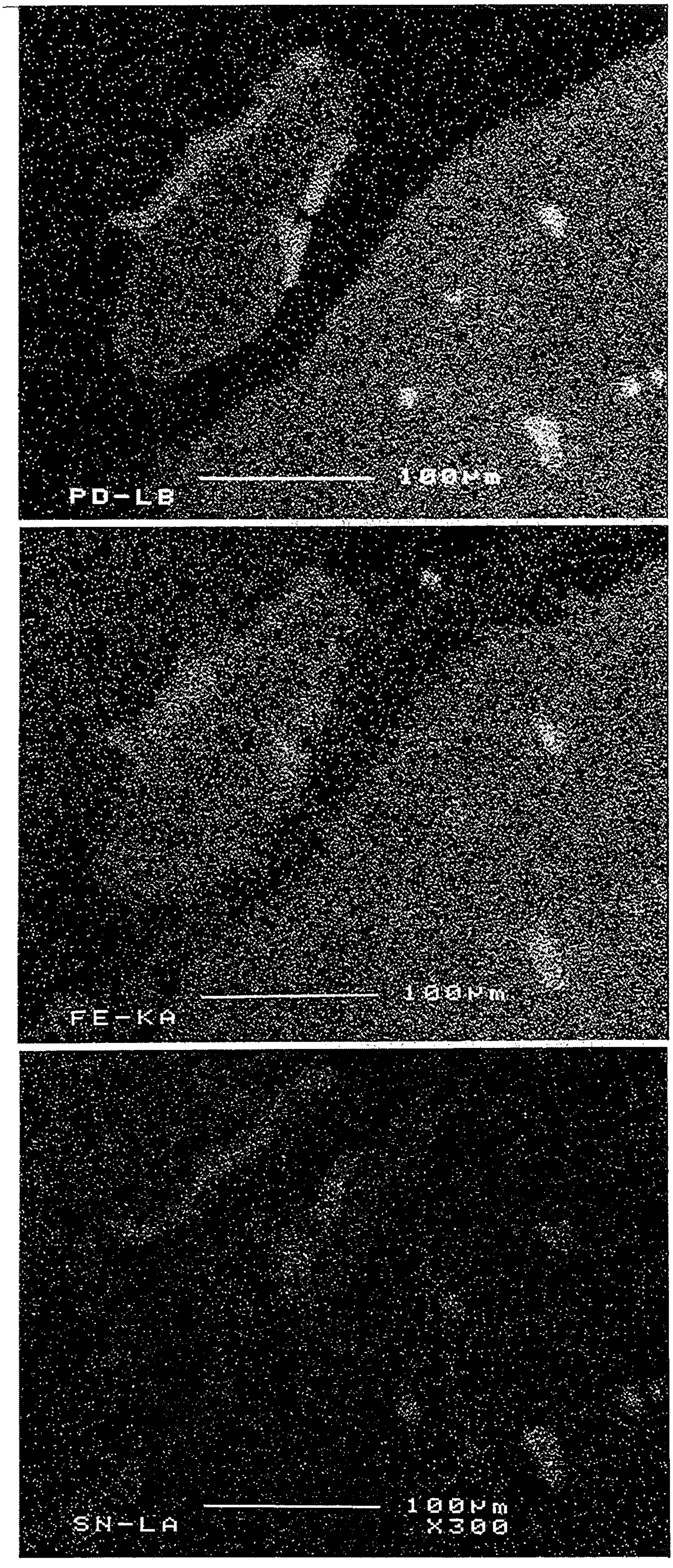

Poussix-04-3
Pos.A

Fig. 17: Continued.

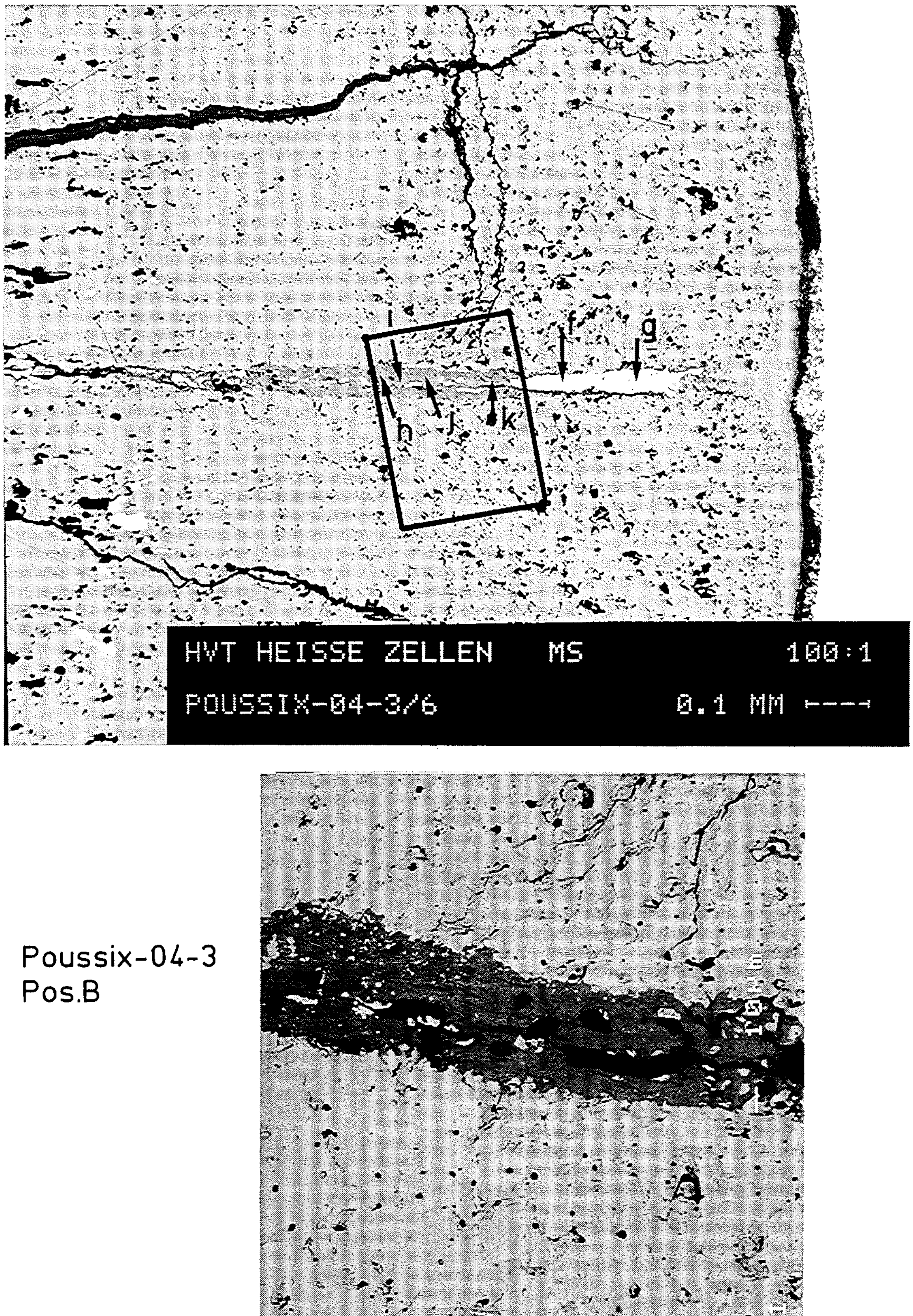

Fig. 18: Light-optical microstructure and backscattered electron image of metallic and ceramic precipitates in a radial fuel crack between 0.7 and 0.9 of the relative fuel radius r/r_o: ε-Ru(Tc, Mo, Fe, Rh, Pd) and (Ba, Sr)·(U, Pu, Zr, RE, Mo)O_3; position B in Fig. 12, see also Table 6.

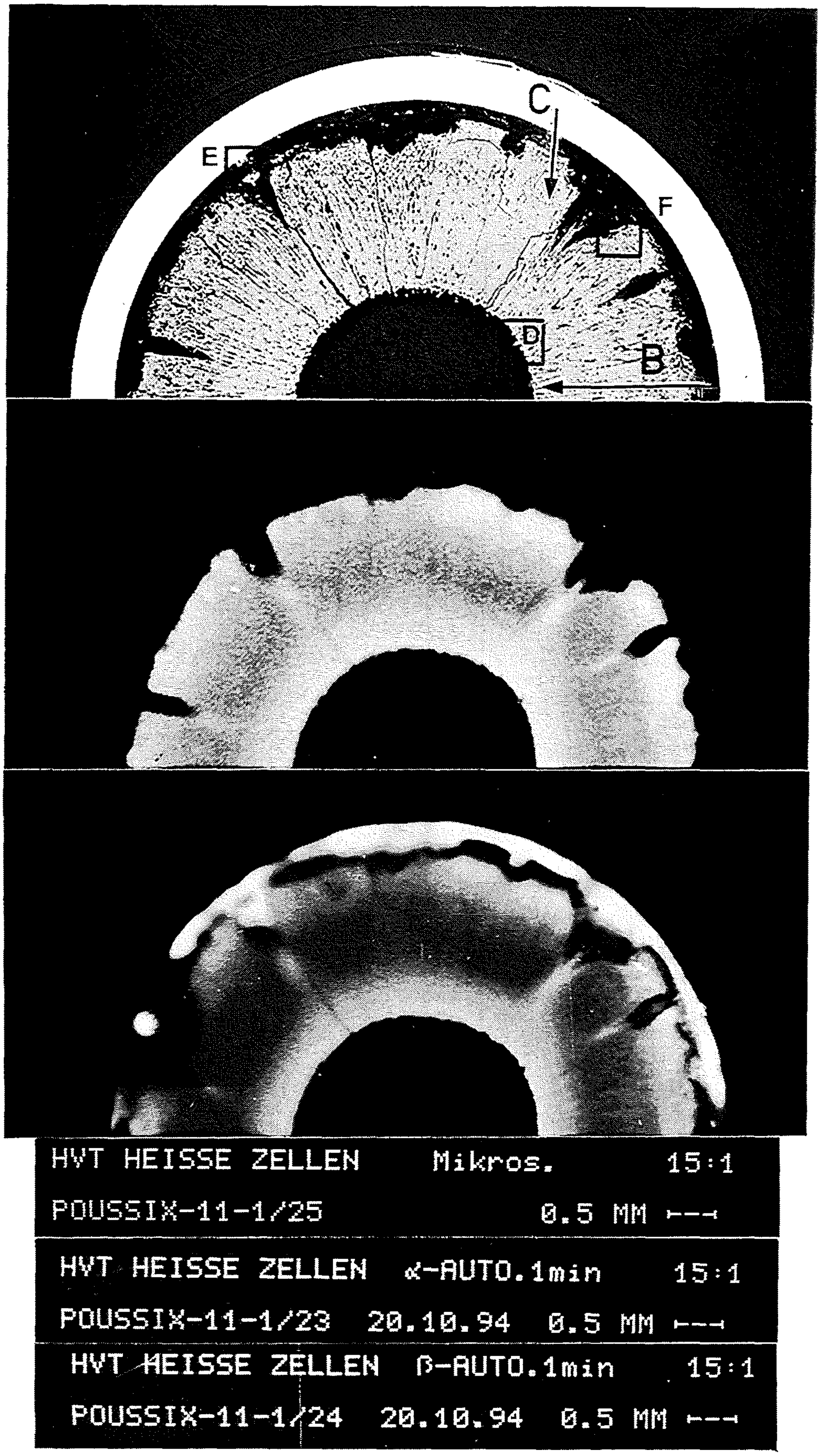

Fig. 19: Microstructure and α- and β-autoradiograph of the half cross-section No. 1, pin No. 11 of the POUSSIX irradiation experiment. Letters indicate the positions of detailed analyses in Figs. 20 to 27.

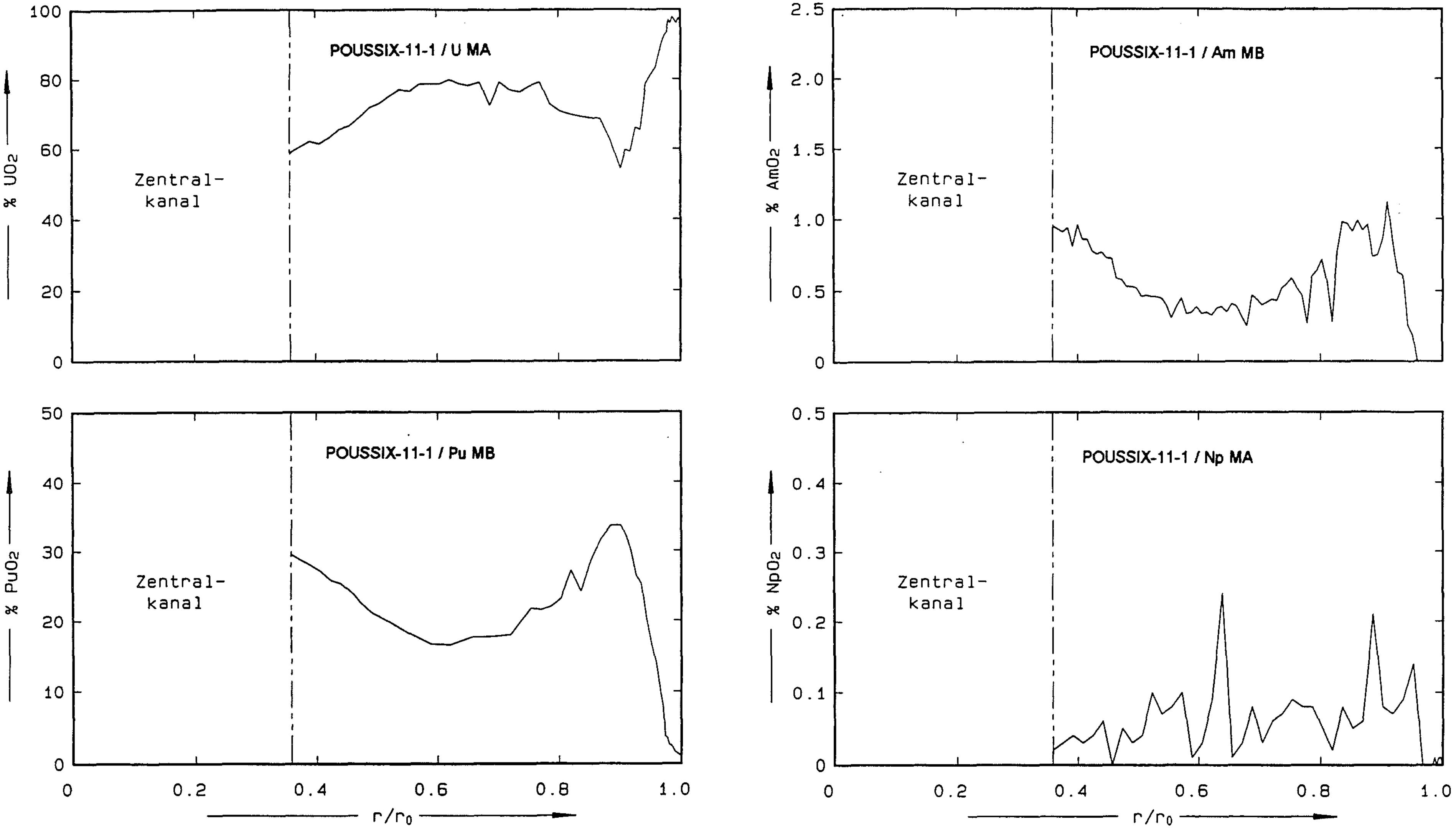

Fig. 20: Radial concentrations of U, Pu, Am and Np (in % MO_2) as a function of the relative fuel radius r/r_o; the central void ZK is on the left side; position B in Fig. 19.

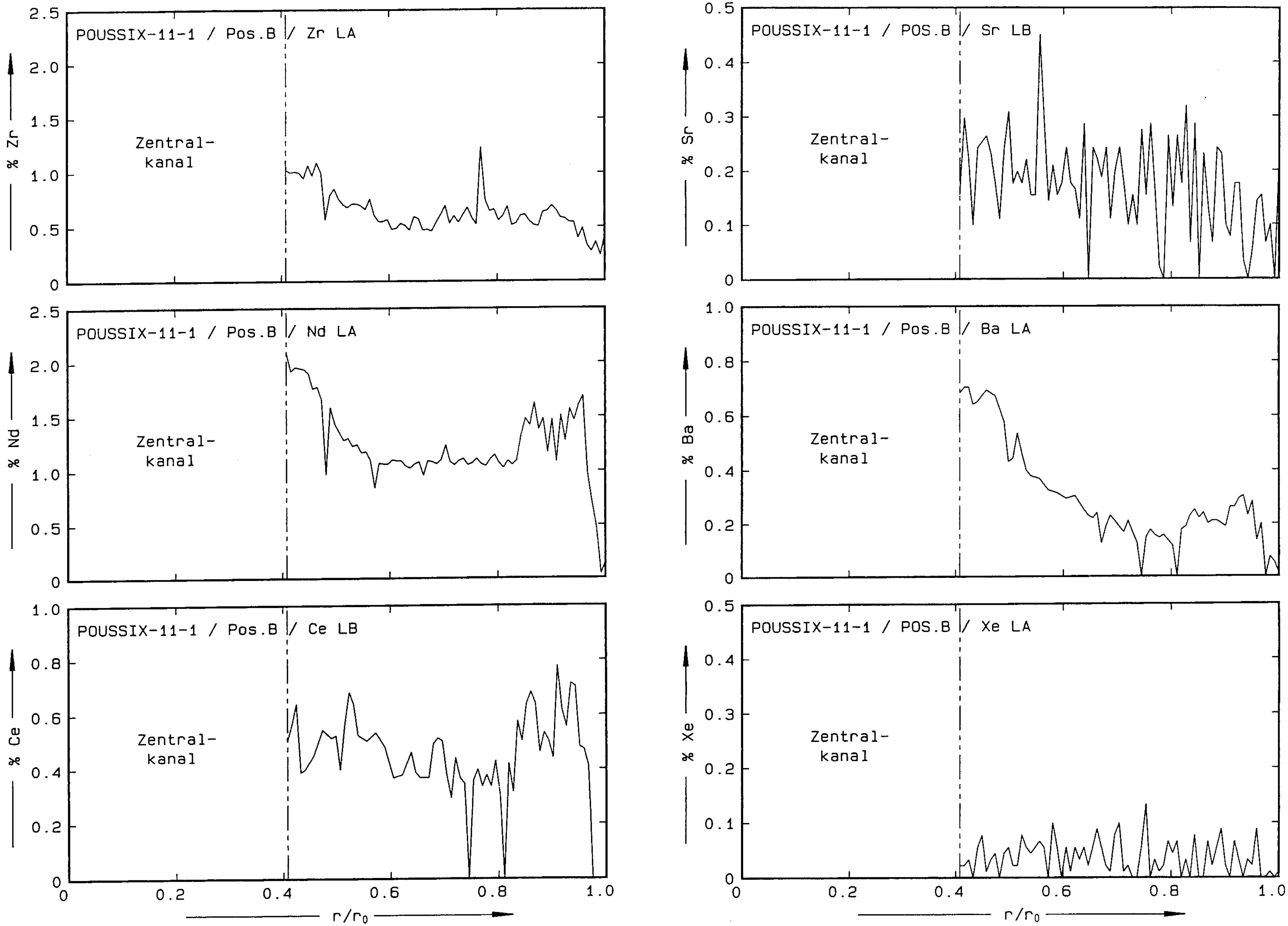

Fig. 21: Radial concentrations of Zr, Nd, Ce, Sr, Ba and Xe as a function of the relative fuel radius r/r$_o$; the central void ZK is on the left side; position B in Fig. 19.

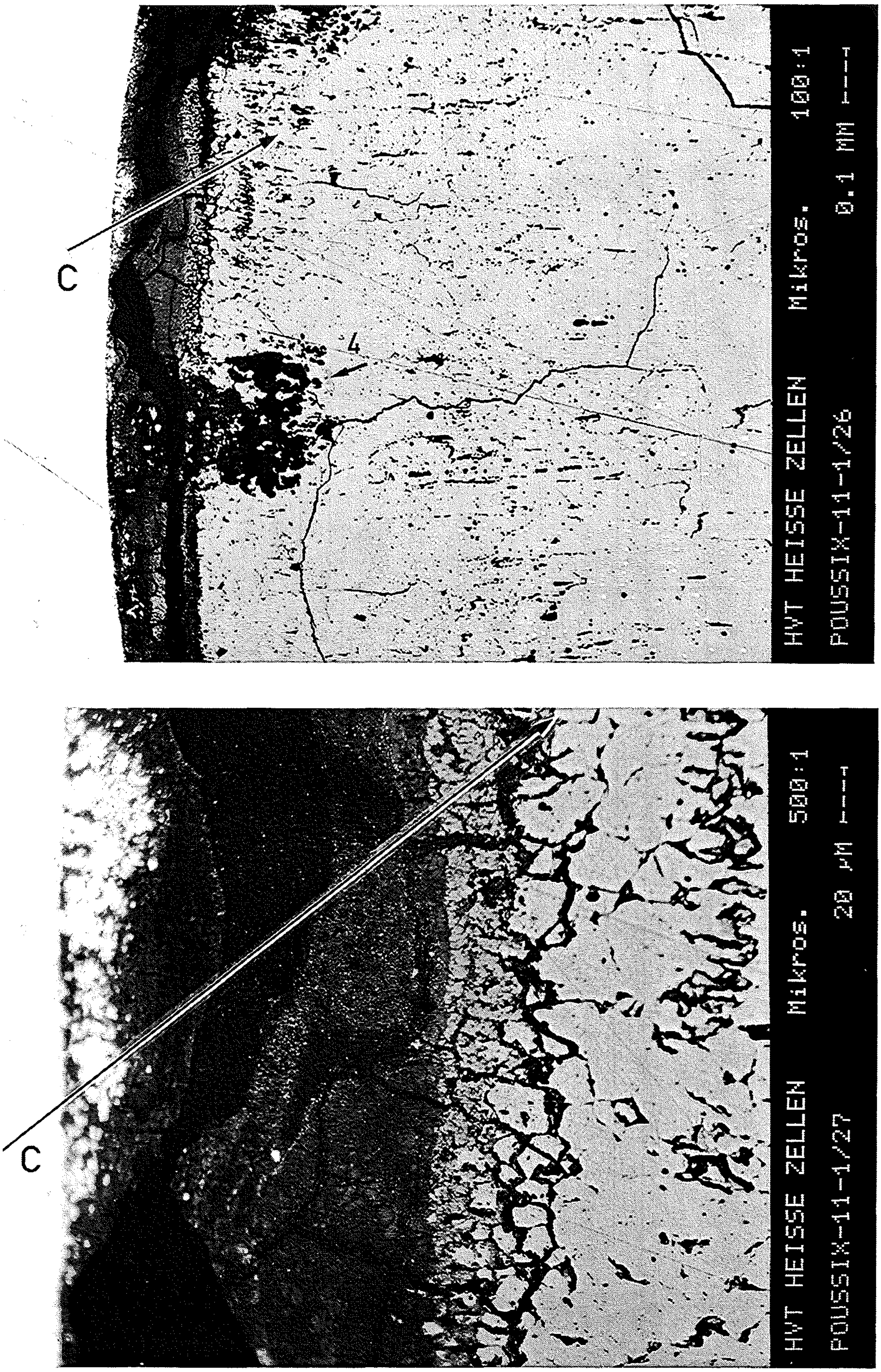

Fig. 22: Light-optical microstructures of the fuel-clad gap. Position C in Fig. 19 denotes the track of the concentration profiles illustrated in Fig. 23. The composition of the ceramic phase 4 is given in Table 7.

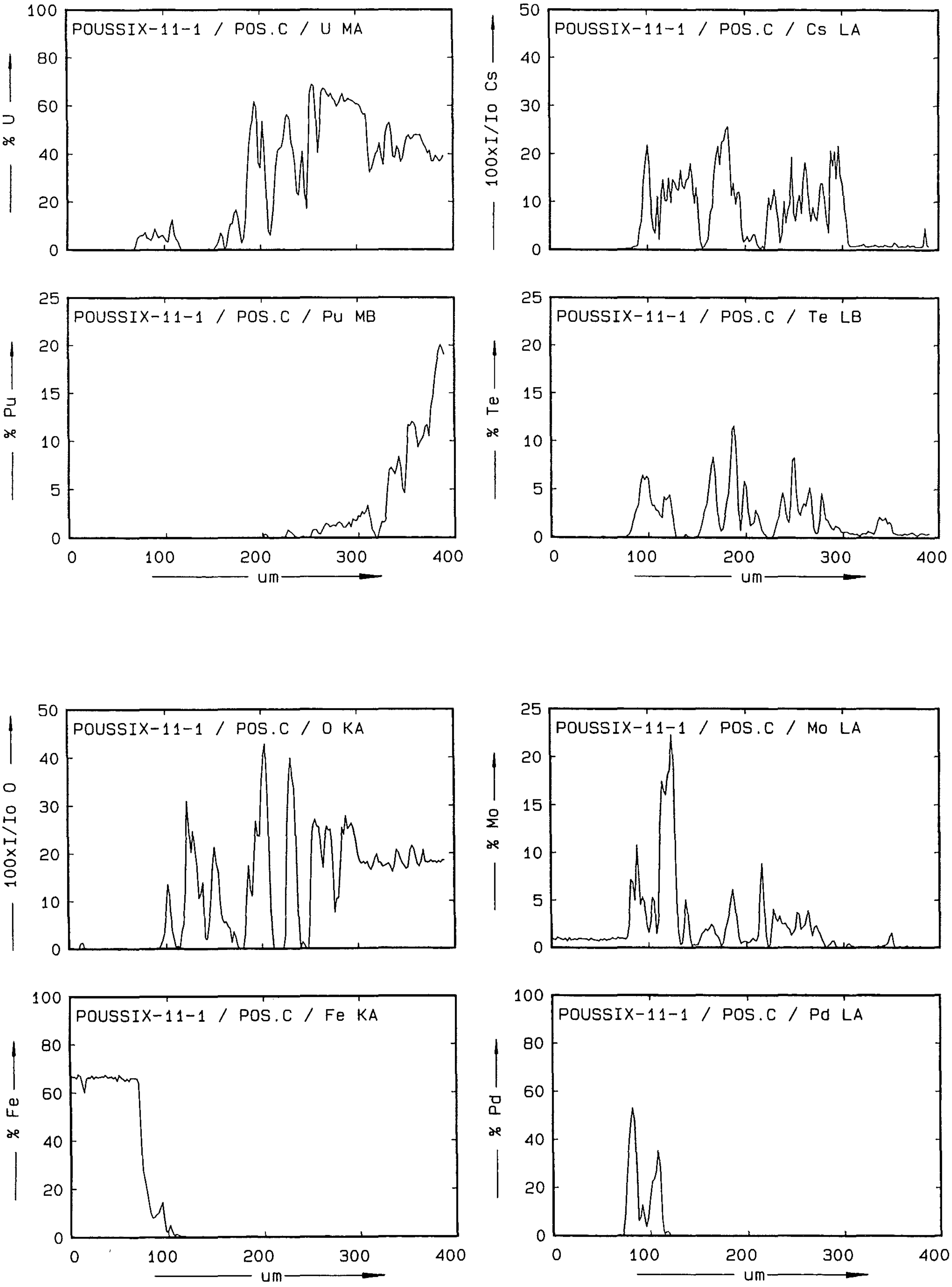

Fig. 23: Concentrations of U, Pu, O, Fe, Cs, Te, Mo and Pd across the fuel-clad gap; position C in Figs. 19 and 22.

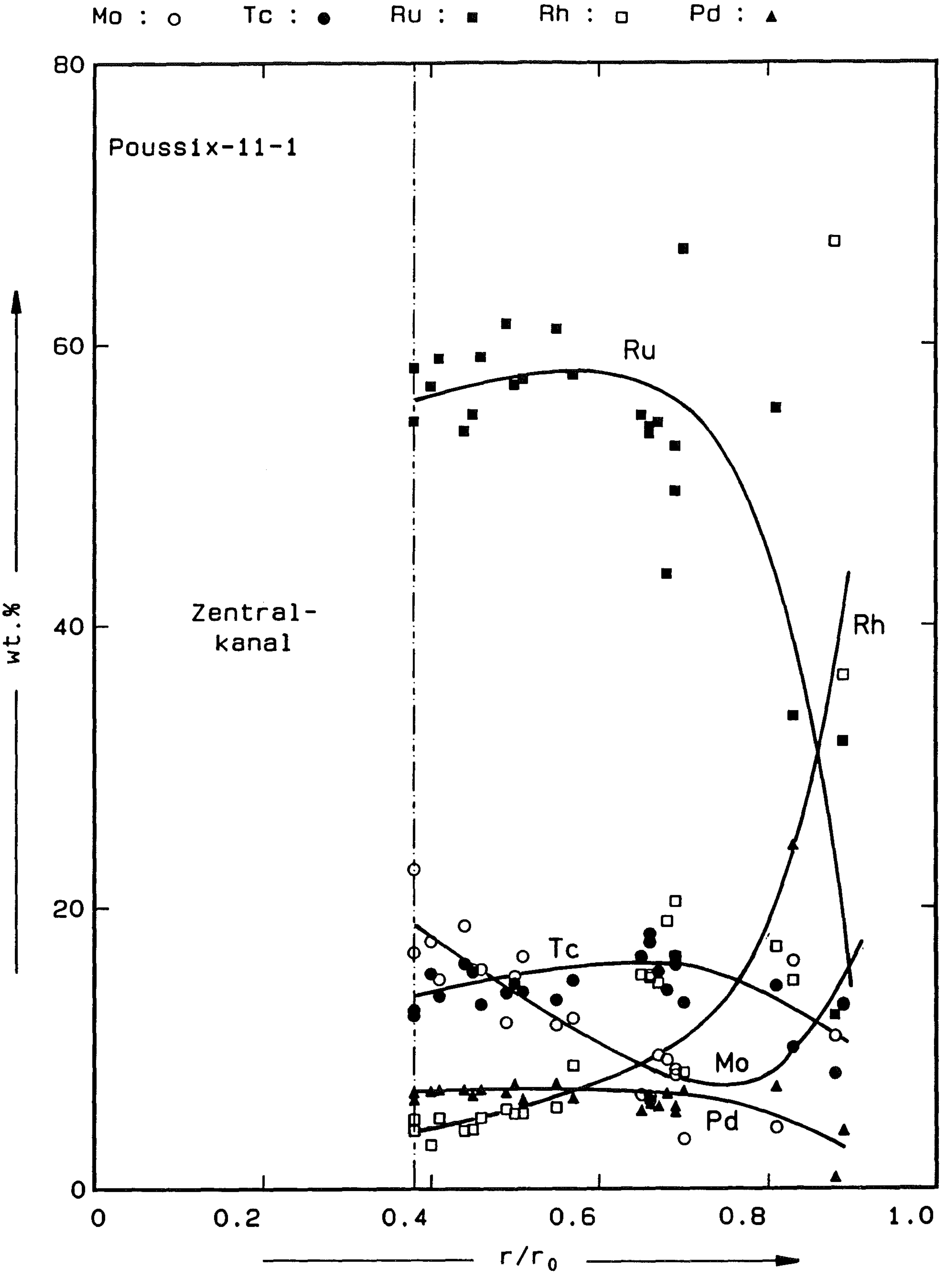

Fig. 24: Composition of the metallic inclusions as a function of the relative fuel radius r/r_0-
The phases are hcp. ε-Ru(Tc, Mo, Rh, Pd).

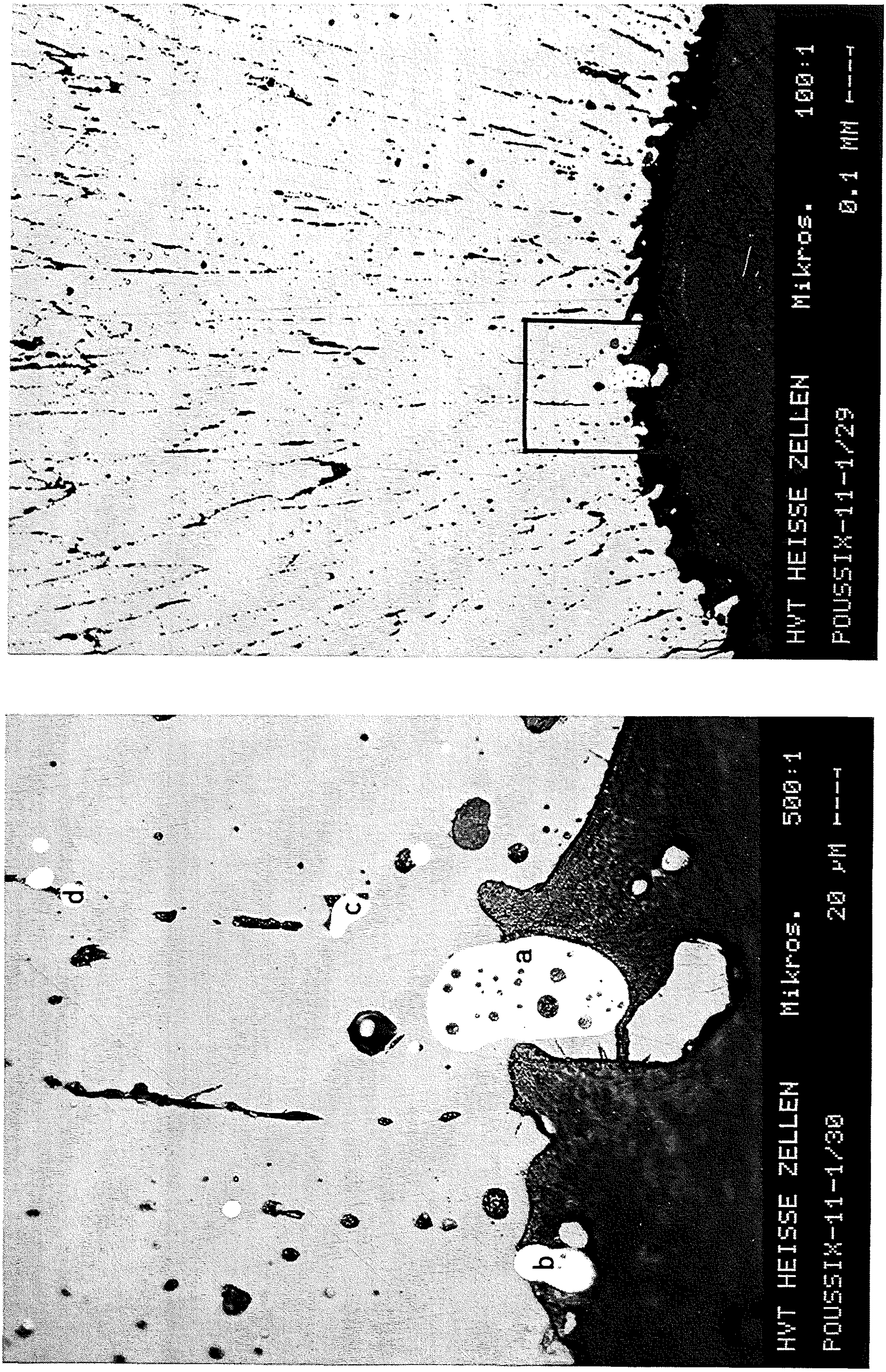

Fig. 25: Light-optical microstructures of metallic precipitates a to d in the fuel near the central void; position D in Fig. 19. The composition of the precipitates is given in Table 5.

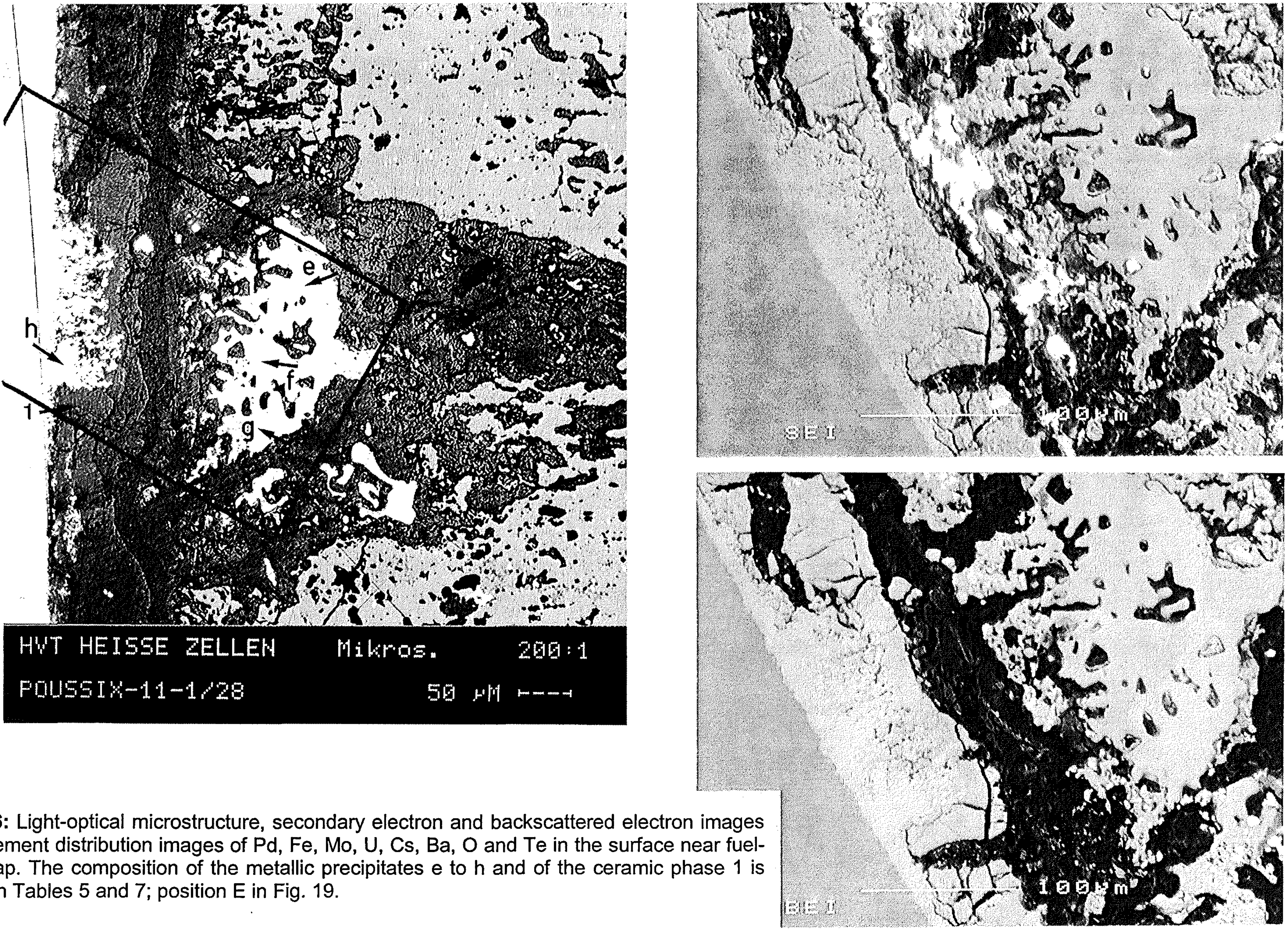

Fig. 26: Light-optical microstructure, secondary electron and backscattered electron images and element distribution images of Pd, Fe, Mo, U, Cs, Ba, O and Te in the surface near fuel-clad gap. The composition of the metallic precipitates e to h and of the ceramic phase 1 is given in Tables 5 and 7; position E in Fig. 19.

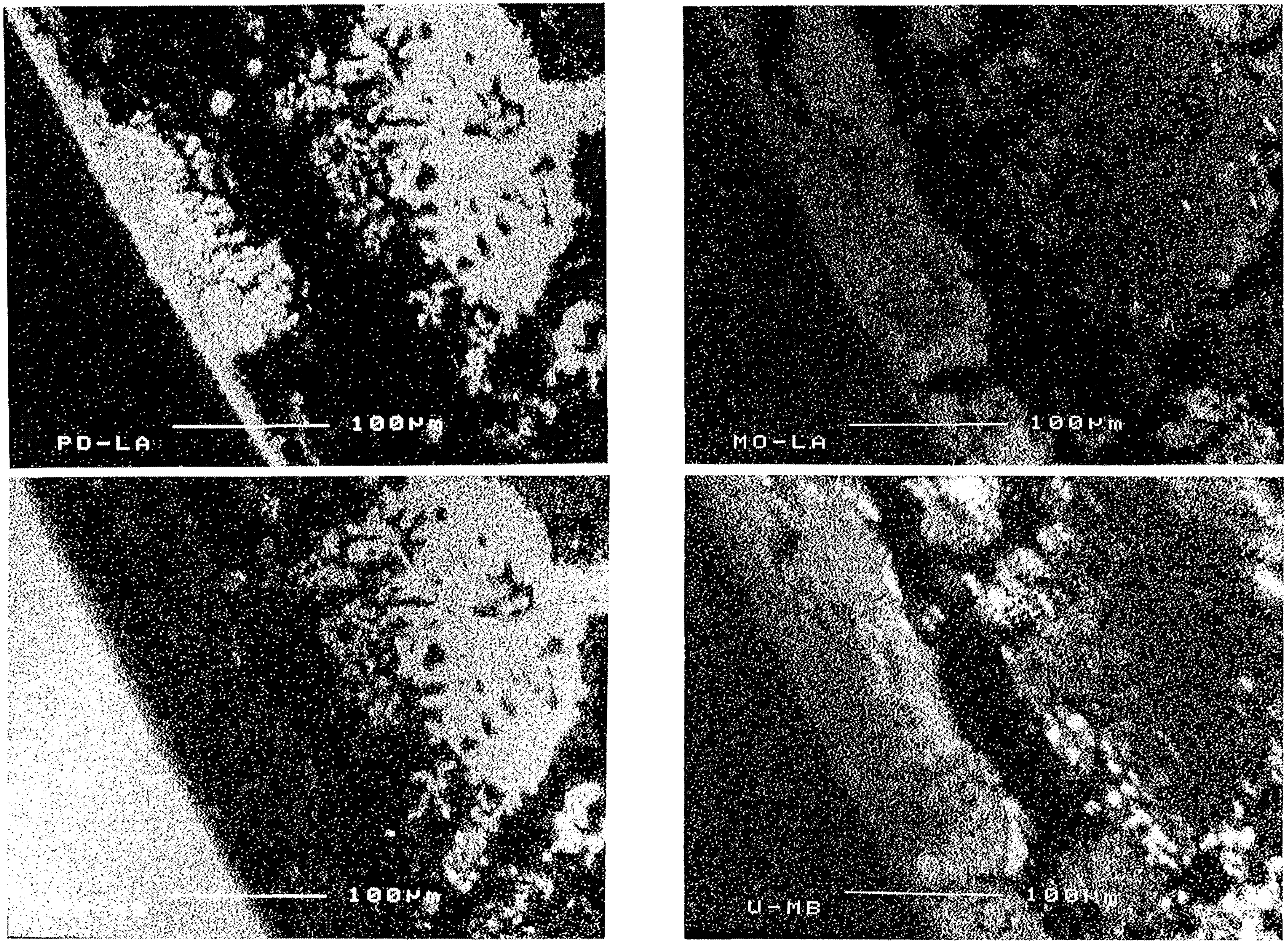

Fig. 26: Continued.

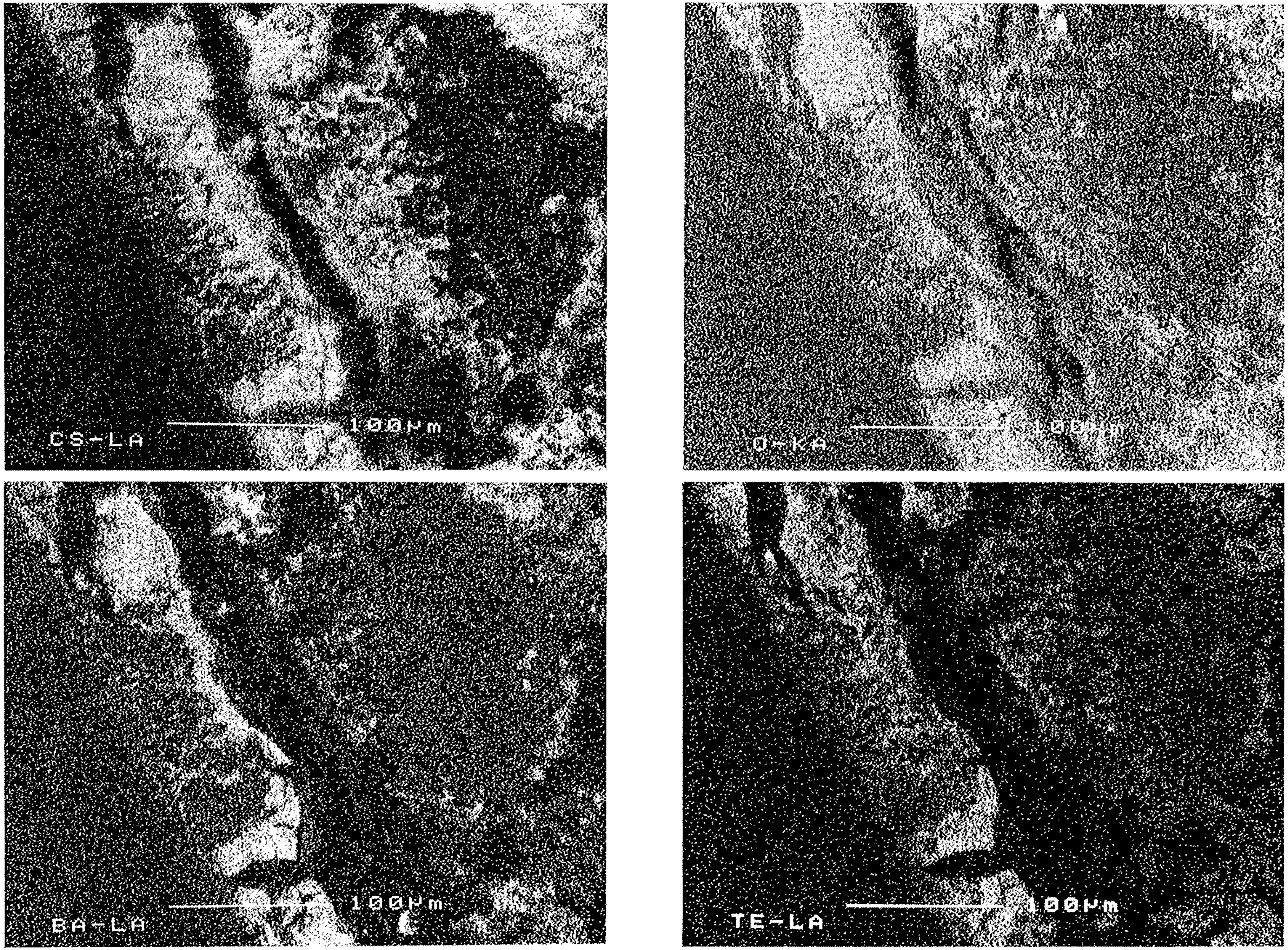

Fig. 26: Continued.

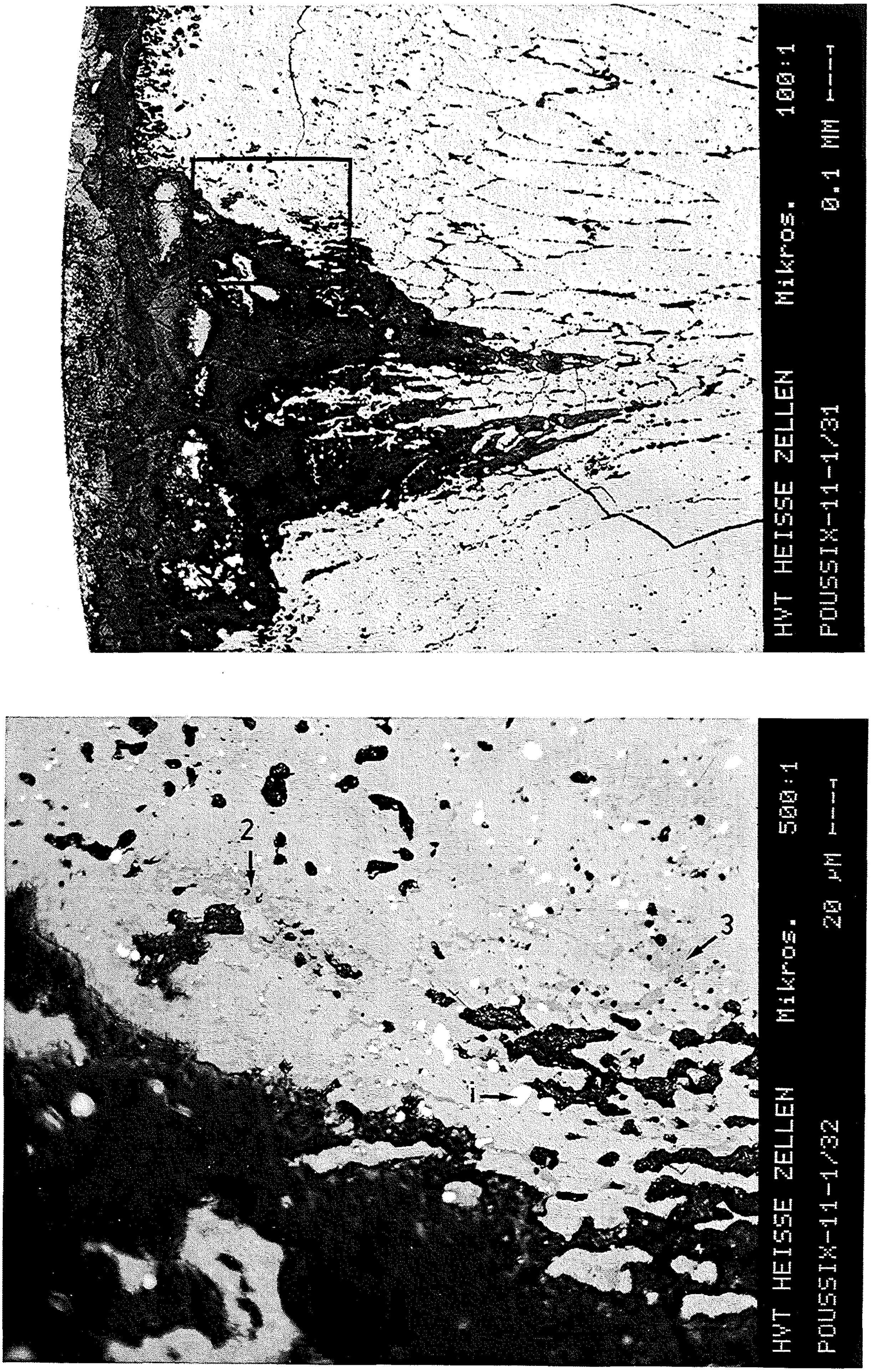

Fig. 27: Light-optical microstructures of precipitates in the surface near fuel region. The composition of the ceramic phases 2 and 3 are given in Table 7; position F in Fig. 19.